Results

In Vitro Vasohibin-1 Release from the Device

Each result is shown as mean ± SD of three different experiments in Figure 1E. A prominent initial increase was observed in vasohibin-1 pellets (Pellet) and it appeared to almost plateau at 7 days after the start of incubation. A minor increase was observed in the vasohibin-1 delivery devices (VDD) with an almost level release observed over the 28 days of incubation. If we examine the amount released from the device (4×4×1.5 mm) between Days 7 and 28, the amount released was estimated to be 0.31 nM/day in the 10VDD group, 0.070 nM/day in the VDD group, 0.088 nM/day in the pellets, and 0 in the NVDD group (Fig. 1E) in a closed incubation system, when we used 500 mg/mL COLs for the permeable PEG/COLs membranes. These calculations were performed from the fitting line between 0 and 28 days. In rat experiments, the release amount would be less, because we used a smaller device for rats than used in the *in vitro* release assay. The larger device used in the *in vitro* release assay in Fig. 1E had 5.44 times (12.25 mm^2 vs 2.25 mm^2) larger drug-releasing surface area and 3.42 times faster releasing rate than that of the transplanted device used in rats, from the results of Fig. S1. The total amount of vasohibin-1 released from the 10VDD devices during the CNV suppression experiment in rats was estimated grossly to be approximately 4.28 nM over 2 weeks. The total amount of vasohibin-1 during the 2 weeks was estimated as about 14.6 nM from the results of Figure 1E, and was divided by 3.42, which is the difference in releasing rate between *in vitro* release assay and *in vivo* experiments, although the effective amount of vasohibin-1 in CNV suppression would be smaller than 4.28 nM, due to drug elimination from the eye. These results were confirmed by western blotting analysis; Figure 1D shows the representative results at Days 1, 7, 14, and 28. A greater amount of vasohibin-1 was observed in the 10VDD and pellet groups than was seen in the NVDD and VDD groups. The results of the pellet group at Day 1 (1d in Fig. 1D) was obtained after diluting the samples five times, because the concentration was too high to be shown by western blotting. However, the size of the pellets was much smaller after 7 days of incubation.

Endothelial Tube Formation

Endothelial tube formation of HUVECs cultured on the NHDF layer was assessed using anti-human CD31 immunostaining (Fig. 2). We used a range of native vasohibin-1 concentrations (from 0 to 10 nM, using 2 nM VEGF) for the preliminary experiments. After the initial examination, the cells were fixed and stained using anti-human CD31. Figures 2A–2G show representative photographs of the experimental results. Figure 2E shows the results of released vasohibin-1 (0.56 nM) from the devices with 2 nM VEGF. Figure 2H shows the average of each experiment; significantly fewer CD31-positive points were observed in released vasohibin-1-treated wells when compared to those of the vehicle released from the NVDD ($p = 0.000001$) or VEGF-treated control ($p = 0.000002$). Vasohibin-1 released from the device showed activity comparable to the native vasohibin-1.

Macro Examination

FD40 was detected in the device (Figs. S2A and S2B show color and fluorescein photographs, respectively) or in pellets (Figs. S2G and S2H) at the implant site through the conjunctiva in the live rats. When we enucleated the eyes at a week after device implantation, mild fibrosis was observed around the devices (Fig. S2C) and around the pellets (Fig. S2I). Fluorescein photography demonstrated the presence of FD40 in the device, with little fluorescein in the conjunctiva and surrounding tissues (Fig. S2D, arrow). FD40 was also detected in the sclera after removal of the device (Figs. S2E and S2F, arrow). Conversely, FD40 pellets showed strong fluorescein on the conjunctiva and surrounding tissues, as was seen for the pellet itself (Fig. S2J, arrow). Furthermore, little fluorescein was observed on the sclera after removal of the device (Figs. S2K and S2L, arrow). Similar conditions were observed when we examined the tissues at 2 weeks after device and pellet implantation; fluorescence was observed over a wider area for those specimens where the device was implanted compared to results at Week 1 (data not shown).

Immunohistology of Vasohibin-1

In immunostained eyes, vasohibin-1-positivity was found in only the 10VDD group (Fig. 3B), but not in the NVDD group (Fig. 3A) or the negative control without the first antibody (Fig. 3D), mainly at the region where vasohibin-1 releasing devices were placed. Pellets showed strong local immunoreactivity, but no immunoreactivity in the retina (Fig. 3C). Vasohibin-1 positivity was observed in the neural retina and optic nerve (white arrows in Fig. 3B). Strong immunoreactivity was observed in the choroid, RPE, and at the inner layer (such as the ganglion cell layer [GCL]) by magnified photographs after device implantation (Fig. 3E).

Leakage from CNV

Fluorescein angiography results of each group at 1 week after the laser CNV procedure are shown in Figure 4A. The results show that an intravitreal injection of vasohibin-1 on Day 4 after the CNV procedure led to a significant reduction of FA scores when compared to those of NVDD ($p = 0.00014$), pellet ($p = 0.020$), and vehicle injection ($p = 0.040$) (Fig. 4B). The 10VDD implantation led to a significant reduction of FA scores when compared to the result of the NVDD group ($p = 0.00006$). The VDD implantation led to a significant reduction of FA scores when compared to those of NVDD ($p = 0.000017$), pellet ($p = 0.012$), and vehicle injection ($p = 0.026$). Although FA scores of the 10VDD group seemed to be smaller than those of the pellet ($p = 0.065$) and vehicle injection ($p = 0.12$), the results were not significant. Figure 5A shows the FA results at Week 2 in each group. Significantly lower FA scores were observed for the vasohibin-1 intravitreal injection group when compared to those of NVDD ($p = 0.000022$), and vehicle intravitreal injection ($p = 0.0065$). Further, significantly lower FA scores were observed in the 10VDD group when compared to those of NVDD ($p = 0.000003$) and vehicle injection ($p = 0.0080$) (Fig. 5B). Significantly lower FA scores were also observed in the VDD group when compared to those of NVDD ($p = 0.000058$) and vehicle injection ($p = 0.011$).

Flat-mount Examination of the CNV Site

Choroidal flat mounts were prepared 2 weeks after device implantation; representative results of each group are shown in Figure 6A. The area of the CNV was 27,288±7,975 μm^2 for the NVDD group; 23,532±13,120 μm^2 for the VDD group; 17,382±715 μm^2 for the 10VDD group; 30,502±780 μm^2 for the vasohibin-pellet group; 26,900±9,067 μm^2 for the intravitreal vehicle injection group, and 12,731±4,113 μm^2 for the intravitreal vasohibin-1 injection group (Fig. 6B). The CNV area was smaller in eyes that were treated with 10VDD or intravitreal vasohibin-1 injection compared to the other treatments. A significantly smaller CNV area was observed in the 10VDD group when compared to those of the NVDD ($p = 0.0004$), pellet transplantation ($p = 0.0011$), and intravitreal vehicle injection groups ($p = 0.000015$). A significantly smaller CNV area was also

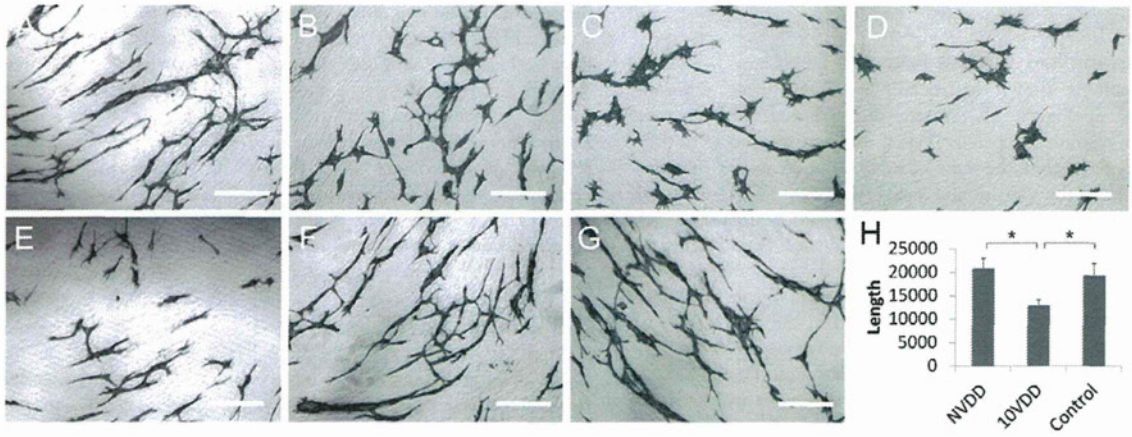

Figure 2. The activity of vasohibin-1 by an endothelial cell tube formation assay. The activity of vasohibin-1 was confirmed by an *in vitro* endothelial cell tube formation assay. Vasohibin-1 suppressed the HUVEC tube formation in a dose-dependent manner. Representative results of HUVEC tube formation treated with 2 nM VEGF combined with 0 (A), 0.2 (B), 2 (C), and 10 nM vasohibin-1 (D) are shown. Bars indicate 100 μm. The released vasohibin-1 from the device showed comparable results to native activity (E). Significant suppression of HUVEC tube formation was observed in released vasohibin-1 when compared to those treated with NVDD (F) and with only 2 nM VEGF without vasohibin-1 (G). (H) shows the average of each experiment; significantly fewer CD31-positive points were observed in released vasohibin-1-treated wells when compared to those of the vehicle released from NVDD ($p<0.0001$) or the VEGF-treated control ($p<0.0001$). The vasohibin-1 released from the device showed activity comparable to the native vasohibin-1. Vertical bar indicates total length of tube formation. NVDD: non-vasohibin-1 (vehicle) delivery device, 10VDD: 10 μM vasohibin-1 delivery device.
doi:10.1371/journal.pone.0058580.g002

observed in eyes injected with intravitreal vasohibin-1 when compared to those of the NVDD ($p = 0.000006$), VDD ($p = 0.0036$), pellet transplantation ($p = 0.000023$), and intravitreal vehicle injection groups ($p = 0.000001$) (Fig. 6B). No significant difference was observed when we compared the VDD with those

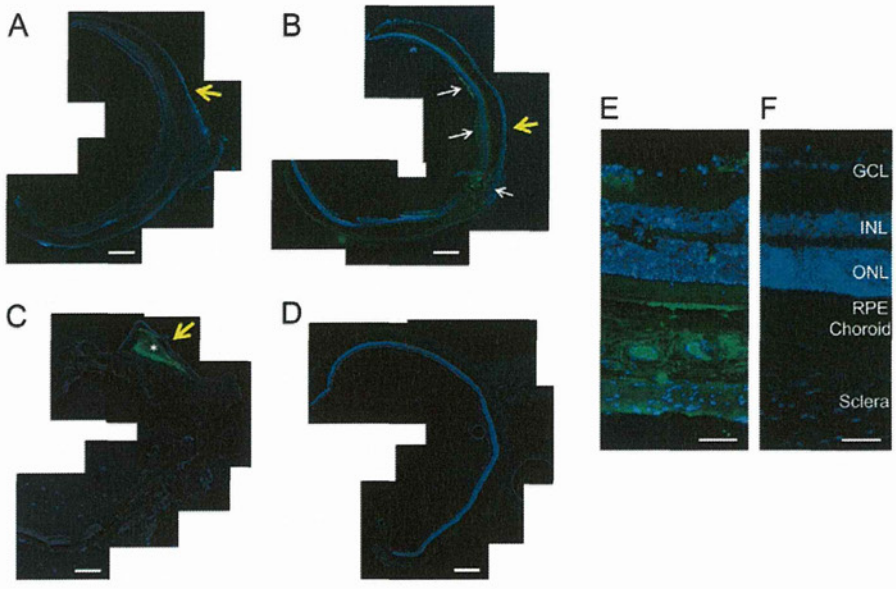

Figure 3. Immunohistochemistry of vasohibin-1 after device implantation. The immunohistochemistry results of vasohibin-1 after NVDD, 10VDD, and pellet implantation are shown. No immunoreactivity was observed after NVDD transplantation (A) and negative control without first antibody (D). 10VDD shows vasohibin-1 immunoreactivity at the device implant area (B). White arrows show the immunoreactivity in the retina and optic nerve at low magnification. Diffuse immunoreactivity was observed in the sclera, choroid, RPE, and retina at greater magnification (E). Strong immunoreactivity was observed in the ganglion cell layer (GCL) and retinal pigment epithelium (RPE), as well as in the sclera and choroid. INL and ONL indicate the inner and outer nuclear layers. These results were not observed in the NVDD group (A) or the negative controls (D and F). Strong immunoreactivity was observed in the pellet (asterisk) and in the tissues surrounding the implanted pellet (C). Yellow arrows indicate the positions where devices or pellets were placed. Devices were removed before sectioning, but pellets were not removed before sectioning. Bars: 200 μm (A–D), and 50 μm (E, F).
doi:10.1371/journal.pone.0058580.g003

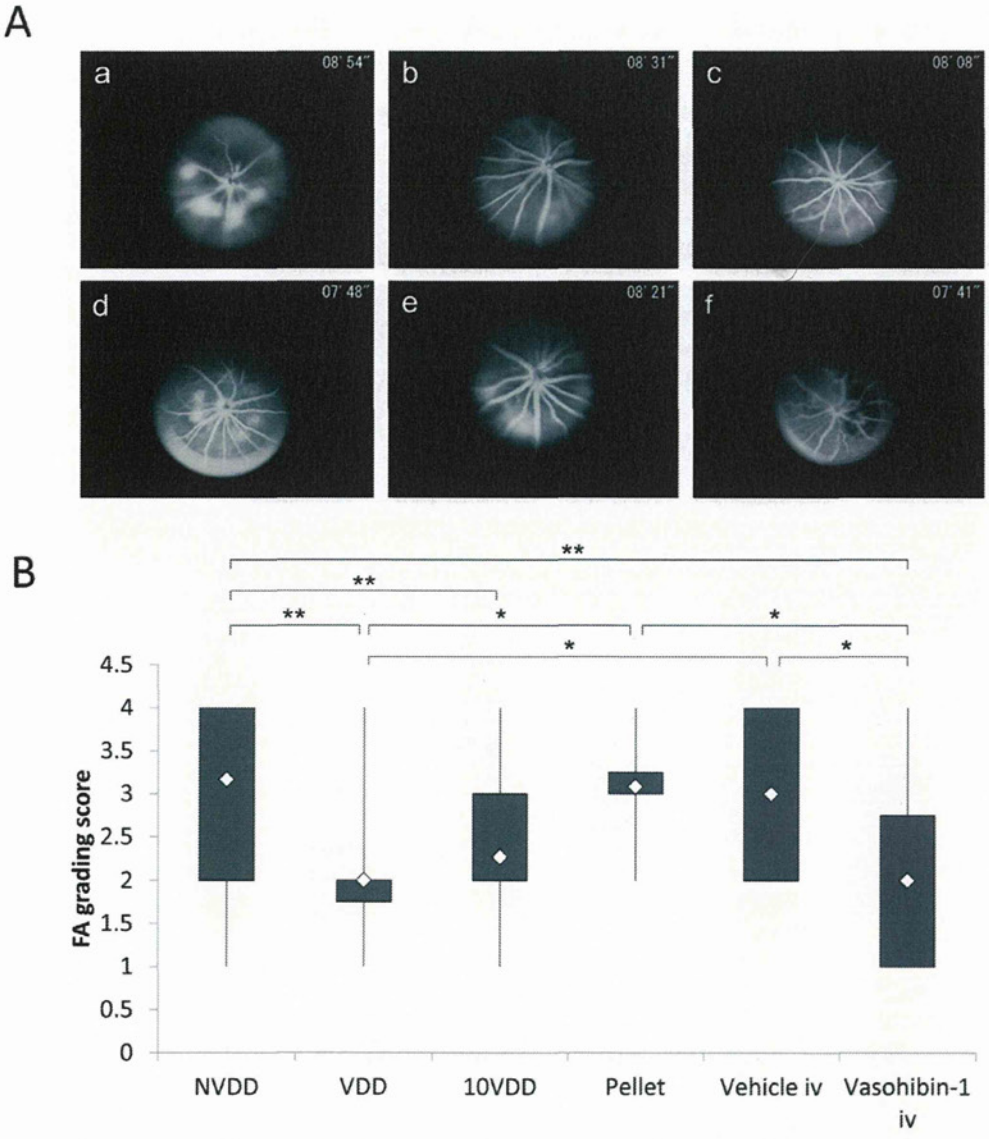

Figure 4. Fluorescein angiography 1 week after CNV laser procedure. (A) Representative results of fluorescein angiography (FA) in each group at 1 week after CNV laser procedure. The groups were treated with NVDD (a), VDD (b), 10VDD (c), vasohibin-1 pellet (d), intravitreal vehicle injection (Vehicle iv) (e), or intravitreal vasohibin-1 injection (Vasohibin-1 iv) (f). (B) Fluorescein angiography scores for each of the six laser spots in each eye are plotted and calculated for each group. Significantly lower FA scores was shown in the Vasohibin-1 iv group when compared to those of NVDD ($p = 0.00014$), pellet ($p = 0.02$), and Vehicle iv ($p = 0.040$). Significantly lower FA scores are also observed in the 10VDD group when compared to the NVDD group ($p = 0.00006$). Significantly lower FA scores are also observed in the VDD group when compared those of NVDD ($p = 0.00017$), Pellet ($p = 0.012$), and intravitreal vasohibin-1 injection ($p = 0.026$). Significant differences are shown as asterisks. NVDD: non-vasohibin-1 (vehicle) delivery device, VDD: 1 μM vasohibin-1 delivery device, 10VDD: 10 μM vasohibin-1 delivery device, Pellet: vasohibin-1 pelletized at the same concentration of 10VDD (without reservoir and cover).
doi:10.1371/journal.pone.0058580.g004

of NVDD ($p = 0.7374$), pellet transplantation ($p = 0.3616$), and intravitreal vehicle injection ($p = 0.7178$) groups.

Discussion

Attention has been paid to sustained drug delivery in the treatment of AMD because regimens including intravitreal anti-VEGF injection require repeated injection and may lead to adverse side effects [9,35]. Sustained delivery of large molecules such as antibodies may be attractive, because not only anti-VEGF therapy and anti-TNFα antibody have shown excellent results in the treatment of refractory eye diseases (such as Behcet's disease), although this regimen also requires repeated cycles of therapy [36,37]. When our devices were cultured in PBS, vasohibin-1 was released over time, with activity equivalent to that seen with native vasohibin-1. These positive results were also observed with brain-derived neurotrophic factor (BDNF) and 40 kDa dextran, as reported previously [24]. Our implantable device showed sustained protein release over time. The relatively large standard

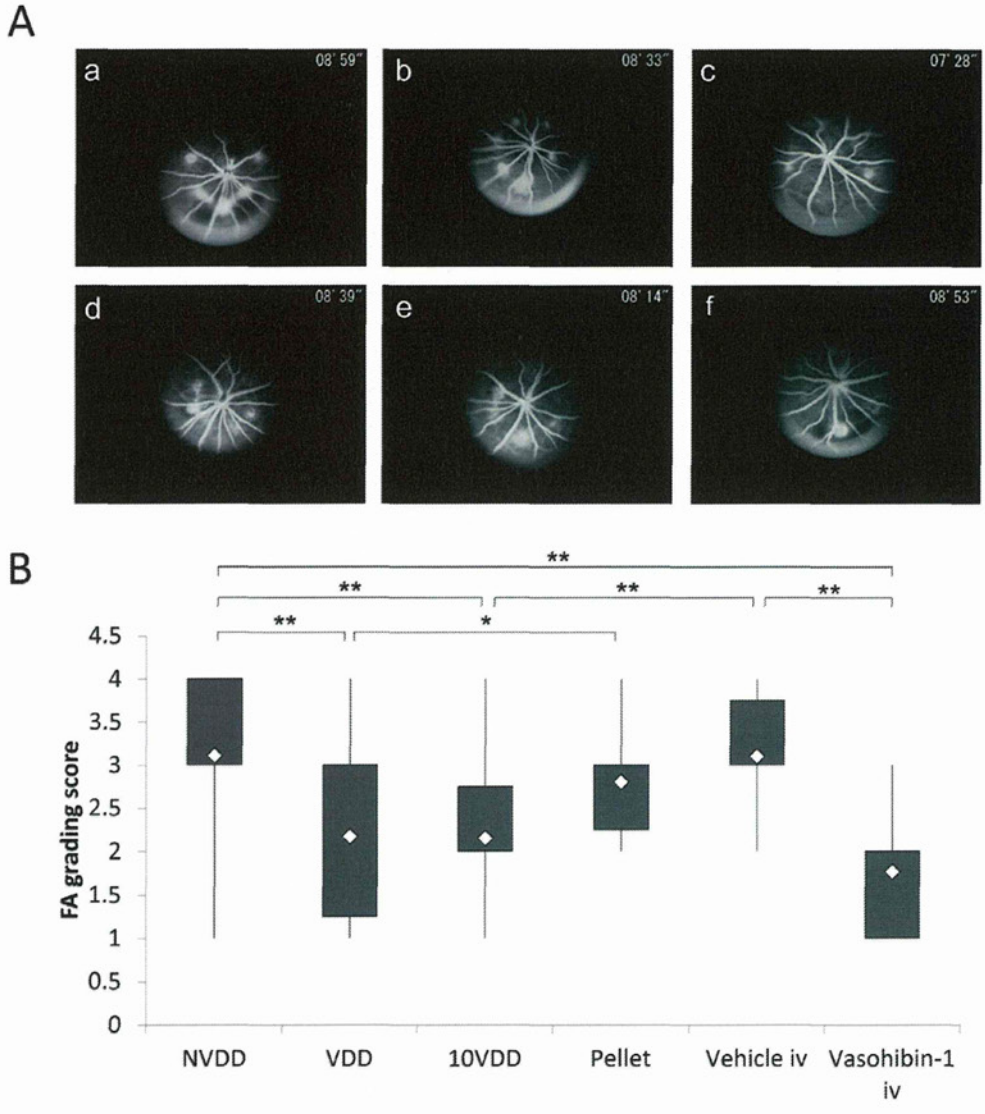

Figure 5. Fluorescein angiography 2 weeks after CNV laser procedure. (A) Representative results of fluorescein angiography in each group at 2 weeks after CNV laser procedure. The groups were treated with NVDD (a), VDD (b), 10VDD (c), vasohibin-1 pellet (d), intravitreal vehicle injection (Vehicle iv) (e), intravitreal vasohibin-1 injection (Vasohibin-1 iv) (f). (B) Significantly lower FA scores was shown in the Vasohibin-1 iv group when compared to those of NVDD ($p = 0.000022$), and Vehicle iv ($p = 0.0065$). Significantly lower FA scores are also observed in the 10VDD group when compared to the NVDD group ($p = 0.00003$) and intravitreal vehicle injection ($p = 0.011$). Significant differences are shown as asterisks. NVDD: non-vasohibin-1 (vehicle) delivery device, VDD: 1 μM vasohibin-1 delivery device, 10VDD: 10 μM vasohibin-1 delivery device, Pellets: vasohibin-1 pelletized at the same concentration of 10VDD (without reservoir and cover).
doi:10.1371/journal.pone.0058580.g005

deviation in the 10VDD group may be indicative of imperfect device preparation. From the results of western blotting, the 10VDD group showed a mild initial release of drug, although the level was far less than seen in the pellet-only group. Technical improvements in delivery device design may overcome these problems. This is an attractive device designed with sustained protein delivery for the treatment of eye diseases.

Subconjunctival drug administration produces better drug penetration than eye drops and is less invasive than intravitreal injection. However, conjunctival and episcleral blood and lymphatic flows have been reported to be the main limiting factors for posterior segment drug distribution by subconjunctival drug administration [38–40]. Our results also showed that implantation of pelletized vasohibin-1 alone (with no reservoir) produced much less vasohibin-1 immunoreactivity than seen with 10VDD implantation. Implanted between the sclera and conjunctiva, our device was designed to release the drugs only to the scleral side of the eye, so a limiting factor of drug diversion to the conjunctival blood flow may be reduced. Carvalho et al [41] reported that their tightly-sutured, one-side-open device delivered higher amount of sodium fluorescein than others, although they used small molecules with their device. From the histological analysis of our experimental procedure, we saw no signs of inflammation or adverse effects in the eye that could be attributed

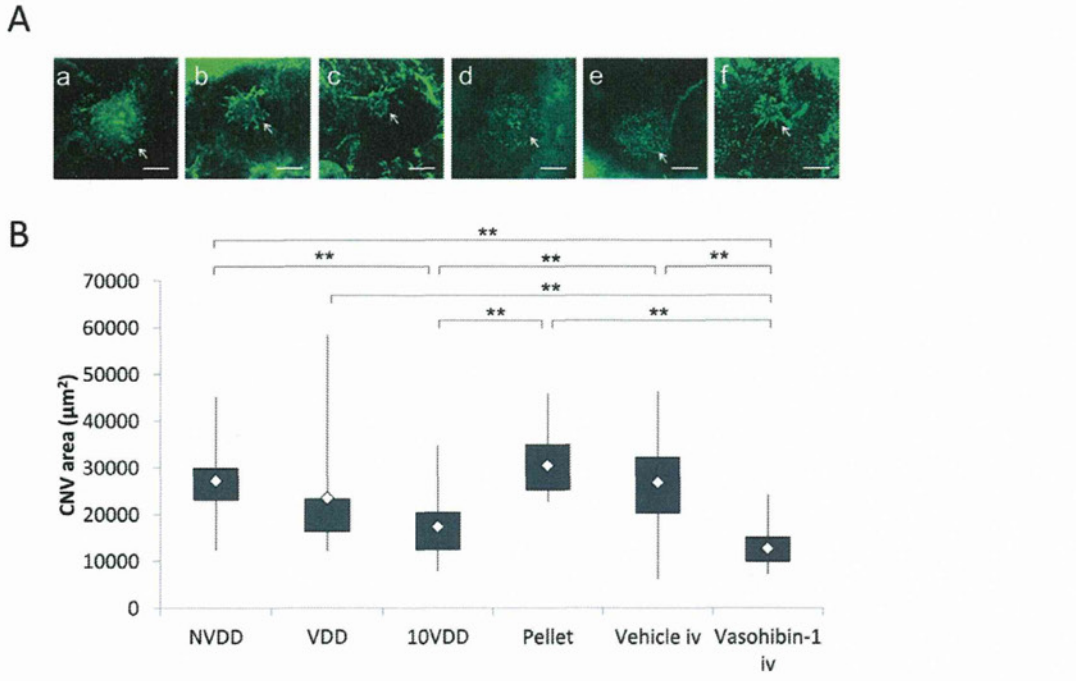

Figure 6. Flat-mount examination of the CNV site. The areas of choroidal neovascularization with devices, pellets, and intravitreal injection of recombinant vasohibin-1 protein. (A) Representative choroidal flat-mount photographs of the groups treated with NVDD (a), VDD (b), 10VDD (c), vasohibin-1 pellet (Pellet) (d), intravitreal vehicle injection (Vehicle iv) (e), intravitreal vasohibin-1 injection (Vasohibin-1 iv) (f) eyes at 2 weeks after the CNV laser procedure. Mean values of actual areas are shown in the text. Bars: 200 μm. (B) Significantly smaller CNV areas were observed in the 10VDD group when compared to those of the NVDD ($p = 0.0004$), Pellet ($p = 0.0011$), and Vehicle iv groups ($p = 0.000015$). Significantly smaller CNV areas were observed in eyes treated with Vasohibin-1 iv when compared to those treated with NVDD ($p = 0.000006$), VDD ($p = 0.0036$), Pellet ($p = 0.000023$), or Vehicle iv ($p = 0.000001$). NVDD: non-vasohibin-1 (vehicle) delivery device, VDD: 1 μM vasohibin-1 delivery device, 10VDD: 10 μM vasohibin-1 delivery device, Pellet: vasohibin-1 pelletized at the same concentration of 10VDD (without reservoir and cover).
doi:10.1371/journal.pone.0058580.g006

to device implantation, except for a mild fibrosis observed around the devices at 2 weeks post-surgery. We also found that the devices removed from the rats where fibrosis was noted showed continuing vasohibin-1 release and comparable activity when we cultured the removed device/tissues in PBS (data not shown).

Vasohibin-1 was observed on the retina at 2 weeks post-implant, principally noted in the regions where the devices were implanted. Some of the regions showed strong immunoreactivity for vasohibin-1, especially at the retinal pigmented epithelium (RPE) and the retinal ganglion cell layer (GCL); the first finding may be due to being the main outer blood-retinal barrier, while the second may be due to the vitreous-retinal barrier [42]. Vasohibin-1 released from the device may be stored in cells in these regions and later released to other regions of the retina or vitreous.

Our results demonstrated that vasohibin-1 can be delivered by our device into the retina transsclerally. Amaral et al also reported transscleral protein (pigment epithelium-derived factor and ovalbumin) delivery into the retina, although they used uncontrollable drug release via a matrix-type implant [10]. Drug released from their device was not delivered unidirectionally. Although there is a blood-retinal barrier, the penetration of such large molecules into the eye may not be so surprising. When we consider the phenomenon of some type of cancer-associated retinopathy, auto-antibodies against retinal cells or retinal-specific antigens have been reported to cause retinal dysfunction [43–45]. The elimination of proteins is reported to be one to two orders of magnitude slower than that of small molecules via the sub-conjunctival and episcleral blood flow [46], with similar results reported for the choroidal blood flow [21]. This fact may also help protein delivery to the retina with the use of our device.

Although we have not studied vasohibin-1 release from the device for more than 2 weeks *in vivo* because of the experimental design, more than 80% of the vasohibin-1 was present in the device at the end of the experimental procedure. The devices removed at the end of the experiment were still releasing vasohibin-1 (data not shown), indicating that it might be possible to use the implanted device for a longer time. These data could also indicate that we may be able to use a smaller device than those used in this experiment to deliver the same amount of drug.

Fluorescein angiography examination showed significantly lower scores in the eyes that received intravitreal vasohibin-1 than those of the intravitreal vehicle-injected eyes. The effects of vasohibin-1 were also confirmed from the flat-mount experiments. These results were same as those previously noted in mice [25]. Our 10VDD device delivered vasohibin-1 to the retina transsclerally, with results comparable to those seen with intravitreal vasohibin-1 injections. With a less invasive method than that of intravitreal injection and the added advantage of continuous drug delivery, our device may be able to replace invasive intravitreal drug injections. Although there was no significant difference between 10VDD and VDD when we evaluated by FA, a statistically significant effect was observed in only 10VDD, but not VDD when we performed the flat-mount examination. One of the reasons these two do not match exactly may be due to the uncertainty about the FA evaluation, as not only blockage by

hemorrhage, but also tissue staining and/or leakage sometimes make evaluation difficult [47]. Further study is needed to determine the exact amounts of vasohibin-1 released from the device, the kinetics of drug distribution, the correlation between drug amount and ocular distribution, and the effects of this regimen on CNV, as well as the appropriate duration of vasohibin-1 release.

Choroidal neovascularization has been reported to be produced by choriocapillaris of the choroidal blood flow [48]. Many effects of choroidal blood flow or RPE may stimulate CNV formation into the retina [49]. Drusen, a preclinical feature of age-related macular degeneration, also stimulates CNV formation [50]. Transscleral anti-CNV drug delivery will be more reasonable than that of intravitreal injection not only from the points of safety, but also from the aspect of CNV pathophysiology. The RPE and RPE-choroid complex are reported to be one to two orders of magnitude slower in drug penetration [21]. When we put our device on the sclera, the drug can pass through the sclera and reach the choroid and RPE earlier than the retina. Between the choroid and neural retina, anti-CNV drugs released from our device may suppress on-going CNV formation. Suprachoroidal bevacizumab was reported to be delivered to the RPE, choroid, and photoreceptors, whereas intravitreal injection distributed more to the inner retina [11]. Olsen et al stressed the importance of delivery of a sustained-release formulation of large molecules to the suprachoroidal space [11]. Our device will offer a safer therapeutic method than those previously reported, especially in the treatment of AMD.

Conclusion

We developed a sustained delivery device for the release of vasohibin-1 in the eye. The released vasohibin-1 showed activity comparable to vasohibin-1 delivered via other methods. When we placed the device on the rat sclera, we found vasohibin-1 released to the sclera, retinal pigment epithelium, and retina. Transscleral vasohibin-1 delivery significantly reduced laser-induced CNV that are comparable as those of effects seen with intravitreal vasohibin-1 injection in the rat eye. Our device will offer a safer therapeutic method than intravitreal injections.

Supporting Information

Figure S1 The size of the devices. The size of the device was 4 mm×4 mm×1.5 mm for the vasohibin-1 releasing assay (A, Device (a)) and 2 mm×2 mm wide ×1 mm high for the rat experiments (A, Device (b)). Because it was very difficult to detect using standard ELISA techniques, we used a larger size device for ELISA. The vasohibin-1 releasing area was 5.44 times larger in Device (a) (3.5 mm×3.5 mm = 12.25 mm^2) than that of Device (b) (1.5 mm×1.5 mm = 2.25 mm^2). Bar: 5 mm. We formulated fluorescein isothiocyanate (FITC) dextran (FD40) as simulated drugs and the device was incubated in a Transwell in 400 μL of PBS at 37°C. To estimate the amounts of FD40 that had diffused out of the Transwells, the fluorescent intensities of the PBS solutions were measured spectrofluorometrically (FluoroscanAscent; Thermo). From the results of a fitting curve (B), we calculated that the releasing rate of the larger device was 0.958 μg/hr/day, whereas the smaller device released 0.28 μg/hr/day; the difference of the releasing rates was calculated as 3.42 (0.958/0.28).
(TIF)

Figure S2 Comparison of FD40DD and FD40 pellet implantations. Rats implanted with FD40DD or FD40 pellets are shown. Devices or pellets were confirmed by color photographs (A and G), after enucleation (C and I), and after device (E) or pellet (K) removal. Mild fibrosis was observed around the devices (C) or pellets (I). FD40 was detected in the device (B), or pellets (H) by fluorescein photography at the site of the implant through the conjunctiva in the live rats during the experiment. When the eyes were enucleated at 1 week after device implantation, little fluorescence was observed in the conjunctiva and surrounding tissues (D, white arrow) in FD40DD-treated rats, whereas strong fluorescence in the conjunctiva was observed in pellet-treated rats (J, white arrow). FD40 was also detected on the sclera after removal of the device (F), but not the pellet (L) (yellow squares indicate the implantation site).
(TIF)

Acknowledgments

The authors alone are responsible for the content and writing of this paper.

Author Contributions

Conceived and designed the experiments: TA NN. Performed the experiments: HO NN HK MN YS NO TN TA. Analyzed the data: HO NN TA. Contributed reagents/materials/analysis tools: NN HK MN TA. Wrote the paper: TA.

References

1. Klein R, Peto T, Bird A, Vannewkirk MR (2004) The epidemiology of age-related macular degeneration. Am J Ophthalmol 137: 486–495.
2. (1986) Argon laser photocoagulation for neovascular maculopathy. Three-year results from randomized clinical trials. Macular Photocoagulation Study Group. Arch Ophthalmol 104: 694–701.
3. Thomas MA, Grand MG, Williams DF, Lee CM, Pesin SR, et al. (1992) Surgical management of subfoveal choroidal neovascularization. Ophthalmology 99: 952–968; discussion 975–956.
4. Eckardt C, Eckardt U, Conrad HG (1999) Macular rotation with and without counter-rotation of the globe in patients with age-related macular degeneration. Graefes Arch Clin Exp Ophthalmol 237: 313–325.
5. Reichel E, Berrocal AM, Ip M, Kroll AJ, Desai V, et al. (1999) Transpupillary thermotherapy of occult subfoveal choroidal neovascularization in patients with age-related macular degeneration. Ophthalmology 106: 1908–1914.
6. (1999) Photodynamic therapy of subfoveal choroidal neovascularization in age-related macular degeneration with verteporfin: one-year results of 2 randomized clinical trials – TAP report. Treatment of age-related macular degeneration with photodynamic therapy (TAP) Study Group. Arch Ophthalmol 117: 1329–1345.
7. Grisanti S, Tatar O (2008) The role of vascular endothelial growth factor and other endogenous interplayers in age-related macular degeneration. Prog Retin Eye Res 27: 372–390.
8. Miller JW, Adamis AP, Shima DT, D'Amore PA, Moulton RS, et al. (1994) Vascular endothelial growth factor/vascular permeability factor is temporally and spatially correlated with ocular angiogenesis in a primate model. Am J Pathol 145: 574–584.
9. Pilli S, Kotsolis A, Spaide RF, Slakter J, Freund KB, et al. (2008) Endophthalmitis associated with intravitreal anti-vascular endothelial growth factor therapy injections in an office setting. Am J Ophthalmol 145: 879–882.
10. Amaral J, Fariss RN, Campos MM, Robison WG Jr., Kim H, et al. (2005) Transscleral-RPE permeability of PEDF and ovalbumin proteins: implications for subconjunctival protein delivery. Invest Ophthalmol Vis Sci 46: 4383–4392.
11. Olsen TW, Feng X, Wabner K, Csaky K, Pambuccian S, et al. (2011) Pharmacokinetics of pars plana intravitreal injections versus microcannula suprachoroidal injections of bevacizumab in a porcine model. Invest Ophthalmol Vis Sci 52: 4749–4756.
12. Martin DF, Parks DJ, Mellow SD, Ferris FL, Walton RC, et al. (1994) Treatment of cytomegalovirus retinitis with an intraocular sustained-release ganciclovir implant. A randomized controlled clinical trial. Arch Ophthalmol 112: 1531–1539.
13. Charles NC, Freisberg L (2002) Endophthalmitis associated with extrusion of a ganciclovir implant. Am J Ophthalmol 133: 273–275.
14. Srivastava S, Taylor P, Wood LV, Lee SS, Robinson MR (2004) Post-surgical scleritis associated with the ganciclovir implant. Ophthalmic Surg Lasers Imaging 35: 254–255.

15. Cashman SM, Ramo K, Kumar-Singh R (2011) A non membrane-targeted human soluble CD59 attenuates choroidal neovascularization in a model of age related macular degeneration. PLoS One 6: e19078.
16. Campochiaro PA, Nguyen QD, Shah SM, Klein ML, Holz E, et al. (2006) Adenoviral vector-delivered pigment epithelium-derived factor for neovascular age-related macular degeneration: results of a phase I clinical trial. Hum Gene Ther 17: 167–176.
17. Chevez-Barrios P, Chintagumpala M, Mieler W, Paysse E, Boniuk M, et al. (2005) Response of retinoblastoma with vitreous tumor seeding to adenovirus-mediated delivery of thymidine kinase followed by ganciclovir. J Clin Oncol 23: 7927–7935.
18. Raghava S, Hammond M, Kompella UB (2004) Periocular routes for retinal drug delivery. Expert Opin Drug Deliv 1: 99–114.
19. Smiddy WE, Smiddy RJ, Ba'Arath B, Flynn HW Jr., Murray TG, et al. (2005) Subconjunctival antibiotics in the treatment of endophthalmitis managed without vitrectomy. Retina 25: 751–758.
20. Yasukawa T, Ogura Y, Tabata Y, Kimura H, Wiedemann P, et al. (2004) Drug delivery systems for vitreoretinal diseases. Prog Retin Eye Res 23: 253–281.
21. Ranta VP, Mannermaa E, Lummepuro K, Subrizi A, Laukkanen A, et al. (2010) Barrier analysis of periocular drug delivery to the posterior segment. J Control Release 148: 42–48.
22. Kunou N, Ogura Y, Yasukawa T, Kimura H, Miyamoto H, et al. (2000) Long-term sustained release of ganciclovir from biodegradable scleral implant for the treatment of cytomegalovirus retinitis. J Control Release 68: 263–271.
23. McHugh AJ (2005) The role of polymer membrane formation in sustained release drug delivery systems. J Control Release 109: 211–221.
24. Kawashima T, Nagai N, Kaji H, Kumasaka N, Onami H, et al. (2011) A scalable controlled-release device for transscleral drug delivery to the retina. Biomaterials 32: 1950–1956.
25. Wakusawa R, Abe T, Sato H, Sonoda H, Sato M, et al. (2011) Suppression of choroidal neovascularization by vasohibin-1, a vascular endothelium-derived angiogenic inhibitor. Invest Ophthalmol Vis Sci 52: 3272–3280.
26. Watanabe K, Hasegawa Y, Yamashita H, Shimizu K, Ding Y, et al. (2004) Vasohibin as an endothelium-derived negative feedback regulator of angiogenesis. J Clin Invest 114: 898–907.
27. Shen J, Yang X, Xiao WH, Hackett SF, Sato Y, et al. (2006) Vasohibin is up-regulated by VEGF in the retina and suppresses VEGF receptor 2 and retinal neovascularization. FASEB J 20: 723–725.
28. Onami H, Nagai N, Machida S, Kumasaka N, Wakusawa R, et al. (2012) Reduction of laser-induced choroidal neovascularization by intravitreal vasohibin-1 in monkey eyes. Retina 32: 1204–1213.
29. Heishi T, Hosaka T, Suzuki Y, Miyashita H, Oike Y, et al. (2010) Endogenous angiogenesis inhibitor vasohibin1 exhibits broad-spectrum antilymphangiogenic activity and suppresses lymph node metastasis. Am J Pathol 176: 1950–1958.
30. Ishikawa Y, Nagai N, Onami H, Kumasaka N, Wakusawa R, et al. (2012) Vasohibin-1 and retinal pigment epithelium. Adv Exp Med Biol 723: 305–310.
31. Tobe T, Ortega S, Luna JD, Ozaki H, Okamoto N, et al. (1998) Targeted disruption of the FGF2 gene does not prevent choroidal neovascularization in a murine model. Am J Pathol 153: 1641–1646.
32. Krzystolik MG, Afshari MA, Adamis AP, Gaudreault J, Gragoudas ES, et al. (2002) Prevention of experimental choroidal neovascularization with intravitreal anti-vascular endothelial growth factor antibody fragment. Arch Ophthalmol 120: 338–346.
33. Yu HG, Liu X, Kiss S, Connolly E, Gragoudas ES, et al. (2008) Increased choroidal neovascularization following laser induction in mice lacking lysyl oxidase-like 1. Invest Ophthalmol Vis Sci 49: 2599–2605.
34. Edelman JL, Castro MR (2000) Quantitative image analysis of laser-induced choroidal neovascularization in rat. Exp Eye Res 71: 523–533.
35. Regillo CD, Brown DM, Abraham P, Yue H, Ianchulev T, et al. (2008) Randomized, double-masked, sham-controlled trial of ranibizumab for neovascular age-related macular degeneration: PIER Study year 1. Am J Ophthalmol 145: 239–248.
36. Sfikakis PP, Theodossiadis PG, Katsiari CG, Kaklamanis P, Markomichelakis NN (2001) Effect of infliximab on sight-threatening panuveitis in Behcet's disease. Lancet 358: 295–296.
37. Ohno S, Nakamura S, Hori S, Shimakawa M, Kawashima H, et al. (2004) Efficacy, safety, and pharmacokinetics of multiple administration of infliximab in Behcet's disease with refractory uveoretinitis. J Rheumatol 31: 1362–1368.
38. Kim H, Csaky KG (2010) Nanoparticle-integrin antagonist C16Y peptide treatment of choroidal neovascularization in rats. J Control Release 142: 286–293.
39. Robinson MR, Lee SS, Kim H, Kim S, Lutz RJ, et al. (2006) A rabbit model for assessing the ocular barriers to the transscleral delivery of triamcinolone acetonide. Exp Eye Res 82: 479–487.
40. Lee SJ, He W, Robinson SB, Robinson MR, Csaky KG, et al. (2010) Evaluation of clearance mechanisms with transscleral drug delivery. Invest Ophthalmol Vis Sci 51: 5205–5212.
41. Pontes de Carvalho RA, Krausse ML, Murphree AL, Schmitt EE, Campochiaro PA, et al. (2006) Delivery from episcleral exoplants. Invest Ophthalmol Vis Sci 47: 4532–4539.
42. Stefansson E, Geirsdottir A, Sigurdsson H (2011) Metabolic physiology in age related macular degeneration. Prog Retin Eye Res 30: 72–80.
43. Kondo M, Sanuki R, Ueno S, Nishizawa Y, Hashimoto N, et al. (2011) Identification of autoantibodies against TRPM1 in patients with paraneoplastic retinopathy associated with ON bipolar cell dysfunction. PLoS One 6: e19911.
44. Thirkill CE, FitzGerald P, Sergott RC, Roth AM, Tyler NK, et al. (1989) Cancer-associated retinopathy (CAR syndrome) with antibodies reacting with retinal, optic-nerve, and cancer cells. N Engl J Med 321: 1589–1594.
45. Chan JW (2003) Paraneoplastic retinopathies and optic neuropathies. Surv Ophthalmol 48: 12–38.
46. Kim SH, Csaky KG, Wang NS, Lutz RJ (2008) Drug elimination kinetics following subconjunctival injection using dynamic contrast-enhanced magnetic resonance imaging. Pharm Res 25: 512–520.
47. Lassota N, Kiilgaard JF, la Cour M, Scherfig E, Prause JU (2008) Natural history of choroidal neovascularization after surgical induction in an animal model. Acta Ophthalmol 86: 495–503.
48. Hayreh SS (2010) Submacular choroidal vascular bed watershed zones and their clinical importance. Am J Ophthalmol 150: 940–941; author reply 941–942.
49. Lutty G, Grunwald J, Majji AB, Uyama M, Yoneya S (1999) Changes in choriocapillaris and retinal pigment epithelium in age-related macular degeneration. Mol Vis 5: 35.
50. Booij JC, Baas DC, Beisekeeva J, Gorgels TG, Bergen AA (2010) The dynamic nature of Bruch's membrane. Prog Retin Eye Res 29: 1–18.

Neurobiology of Disease 48 (2012) 556–567

Contents lists available at SciVerse ScienceDirect

Neurobiology of Disease

journal homepage: www.elsevier.com/locate/ynbdi

Metabolic stress response implicated in diabetic retinopathy: The role of calpain, and the therapeutic impact of calpain inhibitor

Ahmed Y. Shanab [a], Toru Nakazawa [a,*], Morin Ryu [a], Yuji Tanaka [a], Noriko Himori [a], Keiko Taguchi [b], Masayuki Yasuda [a], Ryo Watanabe [a], Jiro Takano [c], Takaomi Saido [c], Naoko Minegishi [b], Toshio Miyata [d], Toshiaki Abe [e], Masayuki Yamamoto [b]

[a] Department of Ophthalmology, Tohoku University Graduate School of Medicine, Japan
[b] Department of Medical Biochemistry, Tohoku University Graduate School of Medicine, Japan
[c] RIKEN Brain Science Institute, Laboratory for Proteolytic Neuroscience, Japan
[d] Division of Molecular Therapy, Tohoku University Graduate School of Medicine, Japan
[e] Division of Clinical Cell Therapy, Tohoku University Graduate School of Medicine, Japan

ARTICLE INFO

Article history:
Received 13 March 2012
Revised 12 July 2012
Accepted 25 July 2012
Available online 9 August 2012

Keywords:
Diabetic retinopathy
Retinal ganglion cell
Calpain
Oxidative stress
Synaptophysin
Neuroprotection

ABSTRACT

To describe how a high fat diet (HFD) and hyperglycemia initiate a sequence of calpain activation and oxidative stress associated with neuro-degenerative changes in diabetic retinopathy (DR), hyperglycemia was induced with streptozotocin in mice lacking the gene for calpastatin (CAST KO), and in mice lacking the gene for the transcription factor NF-E2 related factor 2 (Nrf2 KO). All animals were fed a HFD. Retinal ganglion cell (RGC) density was estimated by labeling with fluorogold and immunohistochemistry. A potent calpain inhibitor, SNJ-1945, was administered daily until the animals were sacrificed. In vitro, oxidative stress-induced RGC loss was evaluated in a high glucose culture medium with and without SNJ-1945. Retinal mRNA of calpain-1 and calpain-2 was measured by quantitative RT-PCR. Pre-apoptotic substrates of cleaved α-fodrin and synaptophysin protein were quantified by immunoblot analysis. Axonal damage was examined in transverse sections of the optic nerve. A HFD and hyperglycemia significantly increased RGC and axonal degeneration 3 weeks into the experiment. Levels of cleaved α-fodrin were increased. In the CAST KO mice, the neurotoxicity was augmented significantly. Gene manipulation of CAST and orally administered SNJ-1945 successfully modified calpain levels in the retina and prevented RGC death. In vitro, a high-glucose culture of retinal cells without antioxidants showed more RGC death than that with antioxidant treatment. The expression of synaptophysin was significantly suppressed by SNJ-1945 treatment. These results suggest that calpain plays a crucial role in metabolic-induced RGC degeneration caused by hyperglycemia and oxidative stress. Antioxidant and calpain inhibition offers important opportunities for future neuroprotective treatment against RGC death in various metabolic stress-induced diseases including DR.

Introduction

Diabetes mellitus (DM) affects approximately 285 million individuals worldwide (Shaw et al., 2010), and in developing countries, over 95% of all cases are type 2 diabetes (Hu, 2011). Around 21% of those patients will have some kind of retinopathy at the first time of diagnosis (Fong et al., 2004). Despite years of clinical and laboratory investigations, diabetic retinopathy (DR) remains the leading cause of blindness among diabetic patients (Resnikoff et al., 2004). Clinical diagnosis of DR still requires detection of vascular pathology, but there is clear evidence that hyperglycemia can cause abnormal neurological manifestations after only 2-weeks (Hancock and Kraft, 2004; Kizawa et al., 2006).

In the clinic, the amplitude of photopic negative response (PhNR), elicited by weak stimuli under dark-adapted conditions and driven mainly by retinal ganglion cells (RGCs) (Frishman et al., 1996), is reduced among diabetic patients, correlated with the degree of optic nerve damage (Kizawa et al., 2006). Measuring the thickness of circumpapillary retinal nerve fiber layer (cpRNFL), which serves as an index for the viability of RGC, with optical coherence topography (OCT), has also been noted to thin with the progress of DR (Costa et al., 2002). Furthermore, asymmetry of the cpRNFL has been observed by OCT in type 2 diabetes patients with no detectable ophthalmoscopical retinopathy (Chihara et al., 1993). At the cellular level, RGCs in postmortem human diabetic retinas have shown increased markers of apoptosis (Abu-El-Asrar et al., 2004). Taken together, this evidence shows that RGCs undergo apoptosis in

* Corresponding author at: Tohoku University Graduate School of Medicine, Department of Ophthalmology, 1-1 Seiryo, Aoba, Sendai, Miyagi 980-8574, Japan. Fax: +81 22 717 7298.
E-mail address: ntoru@oph.med.tohoku.ac.jp (T. Nakazawa).
Available online on ScienceDirect (www.sciencedirect.com).

0969-9961/$ – see front matter © 2012 Elsevier Inc. All rights reserved.
http://dx.doi.org/10.1016/j.nbd.2012.07.025

human eyes with diabetes, leading to a reduction in thickness of the nerve fiber layer. Consequently, it is important to clarify the pathogenesis of RGC death in DR, and develop a neuroprotective treatment to try to rescue RGCs in the early stages of the disease.

In response, we evaluated RGCs in a metabolic model of hyperglycemia, using mice fed a high fat diet (HFD) and given low doses of streptozotocin (STZ), in which low doses of STZ led to partial destruction of pancreatic beta cells and a HFD induced insulin resistance (Mu et al., 2006; Srinivasan et al., 2005). In particular, we examined the contribution of calpain and oxidative stress to hyperglycemia-induced RGC death in vivo and in vitro experiments, and investigated whether modification of the calpain state with a pharmacological inhibitor and or adding of antioxidants has the potential to be a therapeutic target for the treatment of neurodysfunction in patients with DR.

Calpains are a family of 14 calcium-regulated, intracellular cysteine proteases, which modulate cellular functions by limited, specific proteolysis (Huang and Wang, 2001). Expressed ubiquitously in the cytoplasm of mammalian cells, they play an important role in various cell processes, including cell proliferation, signal transduction and apoptosis (Perrin and Huttenlocher, 2002). Calpain-1 (μ-calpain; activated with μM Ca^{2+}) and calpain-2 (m-calpain; activated with mM Ca^{2+}) are the two major calpain isoforms (Goll et al., 2003). Calpains are activated by locally increased intracellular Ca^{2+} levels through calcium channels and intracellular stores (Camins et al., 2006), their domains will shift towards the protease core to form a compact structure (Hanna et al., 2008). It is also associated with the degradation of their substrates including α-fodrin that forms a backbone of the membrane skeleton (Nath et al., 1996), which triggers the apoptosis pathway (Stys and Jiang, 2002).

This makes inhibition of calpain signaling a therapeutic target for several pathological conditions, including DR. Levels of calpain are regulated by an endogenous specific inhibitor, calpastatin. It binds and inhibits calpain when calcium levels are high, but releases it when calcium levels fall (Hanna et al., 2007). Recently, an exogenous calpain inhibitor, SNJ-1945, which has shown a strong ability to penetrate the retinal blood barrier after oral administration (Shirasaki et al., 2005), was described to have a neuroprotective effect against retinal cell degeneration in rat and mouse glaucoma models (Oka et al., 2006; Ryu et al., 2011). In this study, we designed our experiment using mice lacking the gene for calpastatin and SNJ-1945 for investigating the role of calpain activation and possibility of neuroprotection under RGC loss induced by hyperglycemia.

On the other hand, clinical and experimental research in vivo and in vitro in recent years has documented that oxidative stress is a common cause of retinopathy (Hinokio et al., 1999; Pan et al., 2008; Sano et al., 1998). Itoh and his colleagues described how in non-oxidative stress conditions, NF-E2 related factor 2 (Nrf2), a transcriptive factor responsible for regulation of antioxidant response genes, is tethered in the cell cytoplasm by a molecule called Keap-1 and turned over rapidly by proteasomal degradation (Itoh et al., 1999). However, in response to oxidative stress, Nrf2 is stabilized, and relocates to the nucleus, finally activating antioxidant response genes. Therefore, we used mice lacking the Nrf2 gene to induce oxidative stress and evaluate the link between oxidative stress and calpain activation.

The main goal of this study was to develop a better means to identify, prevent and treat DR in its earlier stages rather than wait for the onset of vision-threatening vascular lesions.

Research design and methods

Animals

Adult (10 weeks) male C57BL/6 mice (SLC, Shizuoka, Japan), age- and sex-matched Nrf2 knockout (Nrf2 KO) mice (Itoh et al., 1997), and calpastatin knockout mice (CAST KO) (Takano et al., 2005) were used in this study. All animals were maintained and handled in accordance with the ARVO Statement for the Use of Animals in Ophthalmic and Vision Research and the guidelines from the Declaration of Helsinki and Guiding Principles in the Care and Use of Animals. All experimental procedures described in the present study were approved by the Ethics Committee for Animal Experiments at Tohoku University Graduate School of Medicine.

Mouse model of hyperglycemia

After 4 hr of fasting, hyperglycemia was induced by intraperitoneal injection of streptozotocin (STZ, 40 mg/kg body weight, Sigma, St. Louis, MO) or in the control group, citrate buffer, for five consecutive days. All the animals were fed a high fat diet (405.5 kcal energy, 24.2% protein, 13.6% fat, 3% fiber; Quick Fat, Clea, Japan, INC) at the time of STZ administration and throughout the experiment. Seven days after the first STZ treatment, SNJ-1945 (0.5 mL, 100 mg/kg) (Senju Pharmaceutical Co. Japan, Ltd.) or carboxymethylcellulose (CMC) was administered orally once a day until the animals were killed with an overdose of anesthesia. Blood was sampled from the tail vein and blood sugar was measured with a G-Checker (Gunze, Japan) before and after STZ treatment every week. Body weight was also recorded. Achievement of hyperglycemia was defined by a blood glucose level > 250 mg/dL 7-days after the last injection of STZ, and confirmed by measuring HbA_{1C} 4-weeks after the induction of hyperglycemia.

Retrograde labeling of RGCs and cell count

Retrograde labeling with fluorochrome (Fluorogold: FG, Englewood, CO) was performed as previously described by us (Nakazawa et al., 2007a). Briefly, the mice were anesthetized with a mixture of ketamine (100 mg/kg; Ketaset, Fort Dodge Animal Health, Fort Dodge, IA) and xylazine (9 mg/kg, TranquiVed; Vedco Inc., St. Joseph, MO) prepared at room temperature. Under full anesthesia, two small holes were drilled into the skull at the sites corresponding to the superior colliculi, where 2 μL of 2% FG with 1% dimethylsulfoxide (DMSO) was injected using a Hamilton syringe with a 32 G needle. Seven days after injection of FG, the mice were killed with an overdose of anesthesia; the retinas were harvested, and fixed with 4% of paraformaldehyde (PFA) overnight. The retinas were flat-mounted and the RGC density was determined by counting the FG-labeled RGCs in 12 distinct areas under the microscope (Axiovert-200; Zeiss, Germany) (Nakazawa et al., 2007a).

Quantitative RT-PCR (qRT-PCR)

qRT-PCR was performed as previously described (Nakazawa et al., 2007c) with minor modifications. Neural retinas were sampled and immediately sunk in an RNA stabilization reagent (RNase later, Sample and Assay Technology; Qiagen). Total RNA was extracted from the retinas using an extraction reagent (TRIzol; Invitrogen) and cDNA was synthesized with SuperScript III reverse transcriptase (Invitrogen). Real-time PCR was performed using a 7500 Fast Real Time PCR System (A&B Applied Biosystems, CA) with PCR primers for calpain-1 and calpain-2 designed by TaqMan Gene Expression Assays (Applied Biosystems, Foster, CA). The mRNA levels were normalized to GAPDH as an internal control.

Immunoblot assay

Immunoblotting was performed as previously described with one minor modification (Nakazawa et al., 2007b, 2008). The isolated retinas were placed in a lysis buffer (10 mmol/L Tris–HCl; pH 7.6, 100 mmol/L NaCl, 1 mmol/L EDTA, 1% Triton X-100, protease inhibitors). Each sample

was separated with SDS-PAGE and electroblotted to polyvinylidene fluoride membranes (Millipore, Bedford, MA). After blocking the membrane with 4% skim milk (Bio-Rad Laboratories), the membranes were incubated with a primary mouse monoclonal antibody against α-fodrin (1:1000, Abcam), or a polyclonal antibody against synaptophysin (1:1000, Cell Signaling) and β-tubulin (1:2000, Cell Signaling) overnight at 4 °C. The membranes were then incubated with a horseradish peroxidase-conjugated mouse immunoglobulin secondary antibody followed by avidin–biotin horseradish peroxidase complexes (Vectastain Elite ABC Kit; Vector, Burlingame, CA). The signals were visualized with chemo-luminescence (ECL Blotting Analysis System; Amersham, Arlington Heights, IL) measured by ImageJ software (Ver.1.44, Mac, US) and normalized to β-tubulin.

Immunohistochemistry

Immunohistochemistry (IHC) was performed as previously described (Nakazawa et al., 2007a, 2007b). Briefly, the retinal sections were incubated with a blocking buffer (PBS containing 10% goat serum, 0.5% gelatin, 3% bovine serum albumin, and 0.2% Tween 20) followed by a primary antibody against C38 (BM88) (Wakabayashi et al., 2010) or synaptophysin (1:200; Cell Signaling Technology, Inc.). The sections were then incubated with Alexa 488-conjugated goat anti-mouse or goat anti-rabbit IgG (1:200, Molecular Probes, Eugene) in a blocking buffer. The slides were shielded with a Vectashield mounting medium with DAPI (Vector Laboratories, Burlingame, CA). Photographs of the retina were taken using a

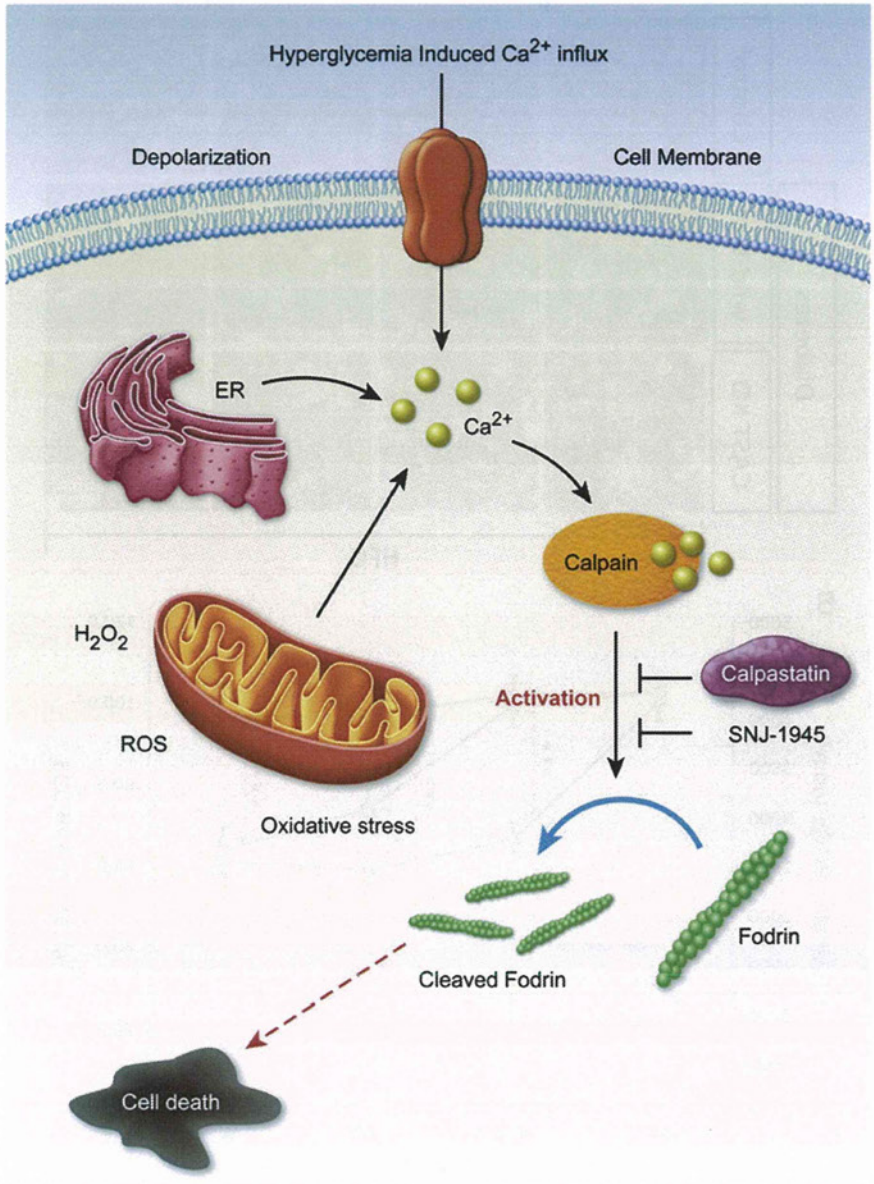

Fig. 1. Illustrative diagram showing the activation of the calpain pathway induced by Ca^{2+} ion influx overload. Hyper-excitability of the cell membrane due to hyperglycemia leads to cell membrane depolarization followed by a Ca^{2+} influx through the voltage sensitive Ca^{2+} channel. Once inside the cell, the excitation of ER and mitochondria through an increase in ROS, and the release of H_2O_2 hints at a release of more intracellular Ca^{2+}, reaching a millimolar level. Subsequently, calpain activation and cleavage leads to cell death. Calpastatin, an endogenous calpain inhibitor, showed the limitations of suppressing calpain activation. On the other hand, SNJ-1945, an exogenous calpain inhibitor, showed a more potential anti-apoptotic effect by suppressing calpain activation in the presence of a pathological intracellular Ca^{2+} level.

microscope equipped with fluorescence illumination (Axiovert-200; Zeiss, Germany).

Histological procedures for optic nerve axon analysis

To investigate the extent of hyperglycemia-induced axonal degeneration, 1 μm sections of optic nerve were processed as described in our previous publications (Nakazawa et al., 2006). Briefly, optic nerves were obtained from animals 4-weeks after STZ-induced hyperglycemia. For quantitative analyses, we analyzed five sections from each experimental condition. Optic nerves were placed immediately into a fixative consisting of 2.5% glutaraldehyde and 2% formaldehyde in 0.1 M cacodylate buffer with 0.08 M $CaCl_2$ overnight at 4 °C. The tissue was washed in 0.1 M cacodylate buffer and post-fixed in 2% aqueous OsO_4. Segments were dehydrated in graded alcohols and embedded in Epon. Then 1-μm sections were cut and stained with 1% toluidine blue in 1% borate buffer. Images were acquired using the 100× oily lens on a light microscope (BX51, Olympus) using a coupled digital camera (MP5Mc/OL, Olympus) and associated DP2-BSW software (Ver.1.3). The acquired images were quantified using Win ROOF software (Ver. 5.8.1). The number of axons was averaged per eye and expressed as numbers/mm^2.

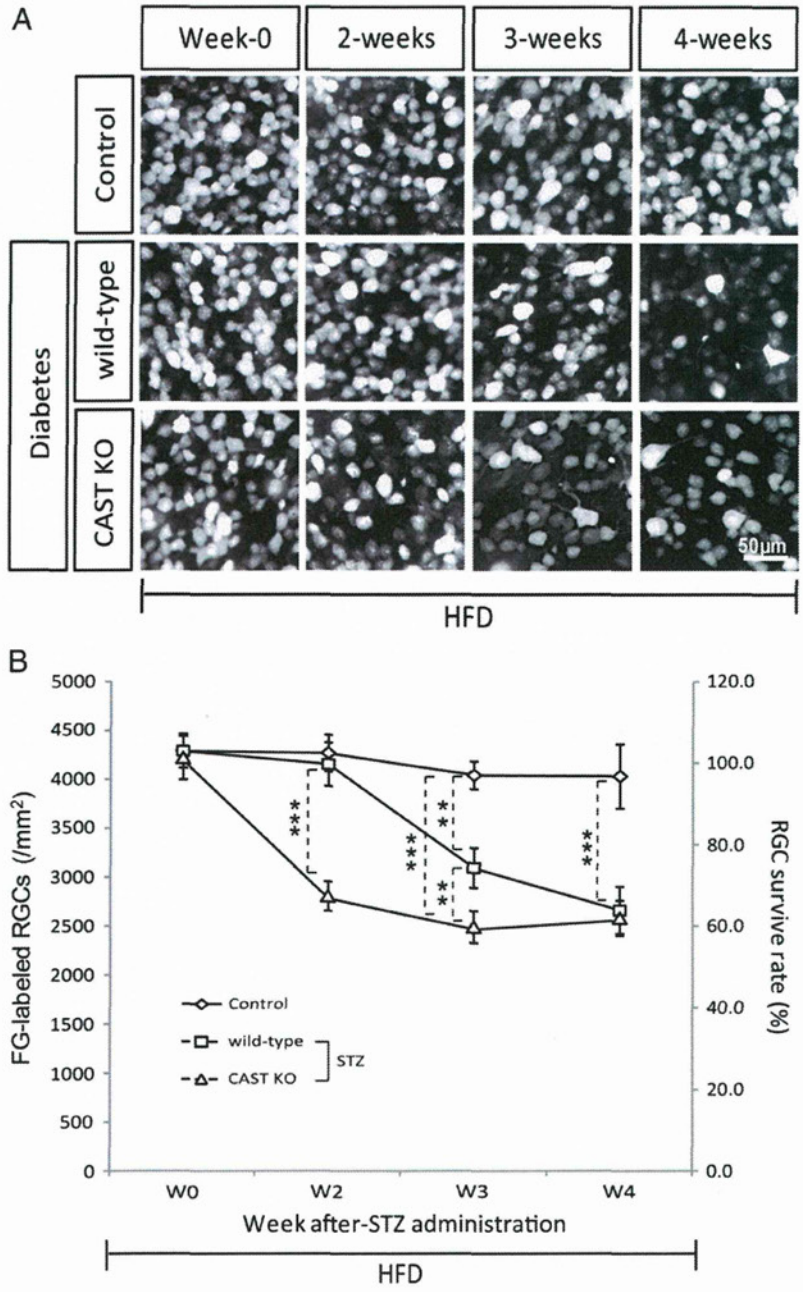

Fig. 2. Time course of fluorogold (FG)-labeled retinal ganglion cells (RGCs) with or without STZ treatment. (A) Representative photos of FG-labeled RGCs in flat-mounted retinas at four different time points (0 weeks: n = 8; two, three, and four weeks: n = 10 respectively). (B) Number of FG-labeled RGCs over time. The quantitative data of FG-labeled RGCs verified the earlier observation that the most significant degeneration was 2-weeks after STZ induction in CAST KO mice, compared to 3-weeks for wild-type mice. This showed the role of calpastatin as an endogenous calpain inhibitor and a limited delay in calpain activation in wild-type mice. Both showed around 38% RGC loss at the fourth week. $^{**}p<0.001$, $^{***}p<0.0001$. Diamonds = control (citrate), squares = wild-type (STZ), triangles = CAST KO (STZ), HFD = high fat diet.

Adult mouse retinal primary cultures

Adult mouse primary retinal cultures were prepared as previously described with minor modifications (Nakazawa et al., 2007a, 2007c). Six neural retinas from 8-week-old mice were immediately dissected in Hank's buffered-saline solution (HBSS) and incubated at 37 °C for 10 min in a CO_2 incubator in a digestion solution containing papain (10 U/mL; Worthington, Lakewood, NJ) and L-cysteine (0.3 mg/mL; Sigma) in HBSS. Retinas were rinsed and triturated in HBSS containing bovine serum albumin (1 mg/mL; Sigma) and DNase (0.2 mg/mL; Sigma). Dissociated cells were passed through a strainer (40-μm nylon net; Falcon, Bedford, MA) and collected by centrifugation. Cells from six mouse retinas were resuspended in a 1 mL Neurobasal A medium (Invitrogen) with B27 supplement without antioxidants (NBA/B27AO−, 10889-038; Invitrogen). The density of retinal cells in the suspension was counted and the cells were seeded to each well of an 8-well chamber (4×10^4 cells per well, Nunc, Naperville, IL, USA). The total volume in each well was increased to 400 μL with NBA/B27AO− or NBA/B27AO+ (antioxidant cocktail = vitamin E, vitamin E acetate, superoxide dismutase, catalase and glutathione; B27, 17504-044; Invitrogen), 1 μg/mL insulin, 2 mM L-glutamate and 12 μg/mL gentamicin with or without 45 mM D-glucose. The cells were further incubated for 24 h with 5% CO_2 at 37 °C with or without 40 μM of SNJ-1945. Cells were then gently washed with PBS and fixed with 4% PFA for 10 min at room temperature. To assess the viability of RGCs, we performed immunocytochemistry (ICC) with mouse anti-βIII tubulin antibody, an RGC marker. The cells were permeabilized with 0.1% Triton X-100 in PBS for 5 min and incubated in a blocking buffer for 30 min at room temperature. Cells were then incubated with a monoclonal anti-βIII tubulin antibody (1:400 dilution, Sigma) at 4 °C overnight, rinsed (PBS 3×, 5 min), incubated with goat anti-mouse secondary antibody (1:200, Alexa Fluor-488; Molecular Probes, 1 hr at room temperature) and rinsed again (PBS 3×, 5 min). Eight-well chamber slides were mounted with a Vectashield mounting medium with DAPI. Controls were treated similarly, except without the primary antibody. Samples were arranged in a pseudo-randomized manner on the plates so that the investigator would not be aware of their identity when quantifying βIII tubulin-positive RGCs. To quantify the βIII tubulin-positive RGCs, 10 random images per well were captured using a fluorescent microscope (20× objective) equipped with a digital imaging system. Subsequently, the βIII tubulin-positive cells were counted using the IMAGEJ software. We repeated these cultures four times; values represent the mean ± SEM of four replicate wells.

Statistical analysis

All data were expressed as mean ± SD. The values were processed for statistical analysis with one-way ANOVA followed by Tukey's post hoc test (JMP, SAS institute, Mac ver.). Differences were considered statistically significant at $p<0.05$.

Results

Induction of hyperglycemia via HFD and STZ

Mice treated with STZ (40 mg/kg, 5 shots/5 days) and fed a HFD showed a significant decrease in body weight, increase in blood sugar levels, and levels of HbA_{1C} (S. Fig. 1). This was true for STZ-treated wild-type, CAST KO, and Nrf2 KO mice compared to age-matched citrate buffer control mice (S. Fig. 1A–D, B–E, C–F).

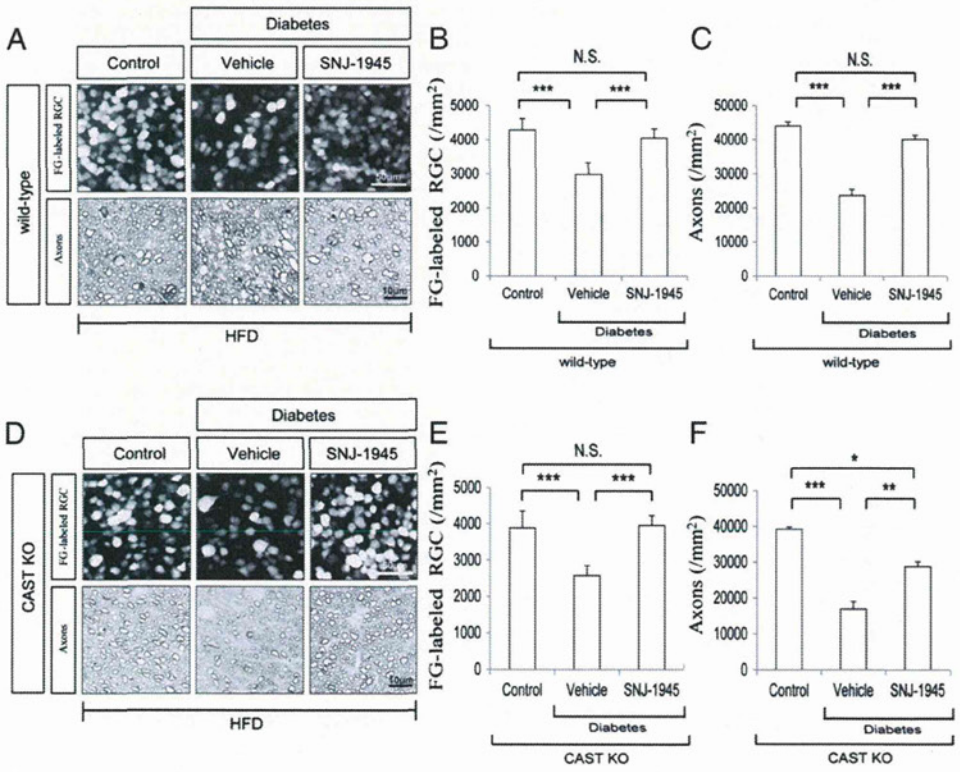

Fig. 3. SNJ-1945 prevented RGC and axonal degeneration in wild-type and CAST KO mice after four weeks of HFD- and STZ-induced hyperglycemia. (A, D upper panels) Representative photographs (wild-type and CAST KO mice, respectively) of FG-labeled RGCs in flat-mounted retinas with or without SNJ-1945 (100 mg/kg/wt). (A, D lower panels) Representative photographs (wild-type and CAST KO mice, respectively) of micro-sectioned samples of the optic nerve axons. (B, E) Bar charts showing quantitative data of the density of FG-labeled RGC in wild-type and CAST KO mice, respectively. (C, F) Bar charts showing quantitative data of axon density in the three different conditions, for wild-type and CAST KO mice, respectively. SNJ-1945 had a significant neuro-protective effect on HFD- and hyperglycemia-induced RGC death and axonal degeneration. N.S.: no significance. *$p<0.01$, **$p<0.001$, ***$p<0.0001$ vs. control.

HbA_{1C} was significantly higher in the mice treated with STZ or SNJ-1945 than in the control mice (S. Fig. 1G, H, I). These data suggest that modification of either calpastatin or Nrf2 does not influence HFD- and STZ-induced hyperglycemia.

HFD- and hyperglycemia-induced RGC death through calpain activation

To investigate the cytotoxic effects of HFD- and STZ-induced hyperglycemia, the density of surviving FG-labeled RGCs was verified at zero, two, three, and four weeks after STZ and in the control group, which received a citrate buffer treatment (Fig. 2). The control group (treated with citrate buffer) experienced no significant change in the density of positive FG-labeled RGCs, but the STZ-treated wild-type mice experienced a significant decrease in the density of FG-labeled RGCs beginning at 3-weeks (3092 ± 204 cells/mm^2, $p = 0.0002$) compared to the control (4041 ± 142 cells/mm^2) at the same time mark. RGC density continued to decline, and at 4-weeks, the percentage of RGCs that survived in the STZ-treated mice was 62.0% (2661 ± 240 cells/mm^2, $p<0.0001$) compared to the control mice (4031 ± 330 cells/mm^2). In STZ-treated CAST KO mice, interestingly, the time scale was different. After only 2-weeks, the density of RGCs was significantly lower (2807 ± 150 cells/mm^2, $p<0.0001$) than in the STZ-treated wild-type mice (4154 ± 222 cells/mm^2) (Fig. 2B). These data suggest that calpain plays an important role in the pathogenesis of RGC death in hyperglycemia-induced retinopathy, and that calpastatin, an endogenous calpain inhibitor, has a limited ability to suppress calpain activation in the retinas of the wild-type mice.

Calpain had a neurotoxic effect on HFD- and hyperglycemia-induced RGC death and axonal degeneration

To investigate whether calpain activation played a role in HFD- and hyperglycemia-induced degeneration of RGCs and their axons, we sampled the retina and optic nerve 4-weeks after STZ treatment. The density of positive FG-labeled RGCs was significantly lower (2985 ± 345 cells/mm^2, $p<0.0001$) in the wild-type mouse vehicle (STZ-CMC) group compared to the control group treated with citrate buffer (4289 ± 330 cells/mm^2). Orally administered SNJ-1945 significantly (4051 ± 269 cells/mm^2, $p<0.0001$) suppressed the degeneration of RGCs (Fig. 3A, upper panel, B) compared to the vehicle group. Concomitantly, axonal degeneration was significantly ($40{,}072 \pm 1192$ axon/mm^2, $p<0.0001$) suppressed in STZ-SNJ-1945 treated mice, compared to the vehicle group ($23{,}656 \pm 1798$ axon/mm^2) (Fig. 3A, lower panel, C). In the CAST KO mice, the density of RGCs degenerated significantly (2580 ± 271 cells/mm^2, $p<0.0001$) in the vehicle group compared to the control group mice (3890 ± 461 cells/mm^2). SNJ-1945 was also able to suppress the degeneration of RGCs (3959 ± 275 cells/mm^2, $p<0.0001$) (Fig. 3D, upper panel, E) and their axons ($28{,}742 \pm 1427$ axon/mm^2, $p<0.0001$) (Fig. 3D, lower panel, F) compared to the vehicle group. These data showed a coincident degeneration of both RGCs and their axons after

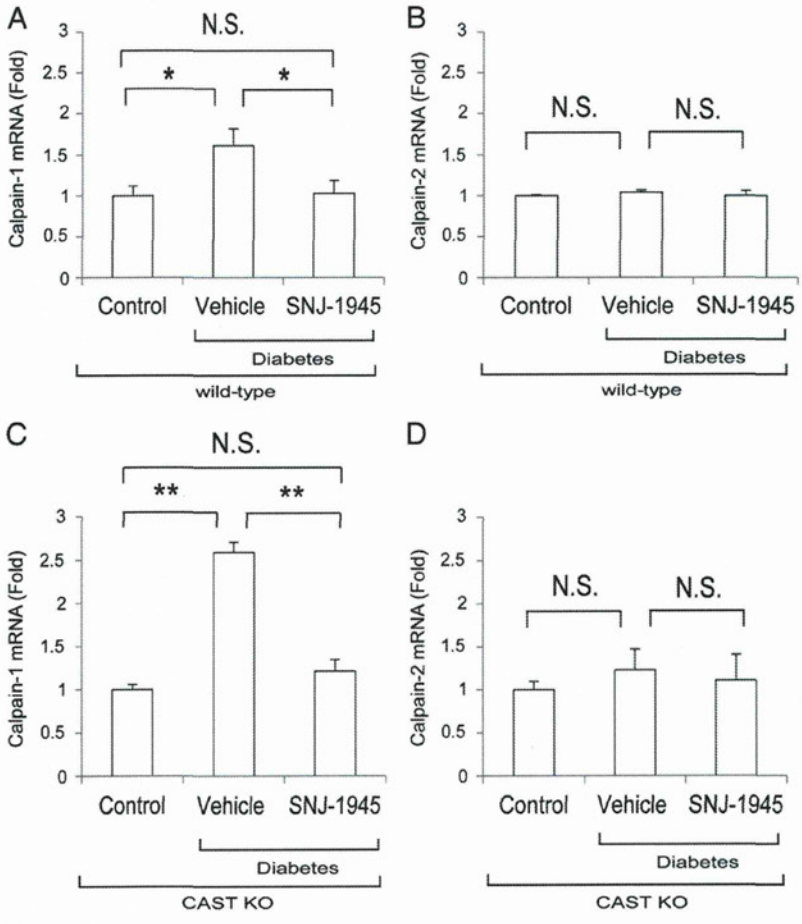

Fig. 4. Calpain-1 but not calpain-2 was activated in HFD and STZ-induced hyperglycemia. (A–B wild-type mice; C–D CAST KO mice) Bar charts showing the quantitative data from qRT-PCR in the neural retina with specific primer sets for calpain-1 and calpain-2 4-weeks after HFD- and STZ-induced hyperglycemia ($n = 6$ each condition). N.S.: no significance. *$p<0.05$, **$p<0.01$ vs. control.

4-weeks of HFD- and STZ-induced hyperglycemia. Combined with higher neuro-degeneration in the CAST KO mice compared to the wild-type mice, this indicated that calpain is a leading cause of RGC death in HFD–hyperglycemia induced retinopathy, and that SNJ-1945 protected RGCs and their axons in both diabetic wild-type and CAST KO mice.

HFD- and hyperglycemia-induced calpain activation in mouse retinas

To investigate the role of the calpain pathway in the retina, we evaluated the gene expression in our model of calpain-1 and calpain-2 in the retina 4-weeks after treatment with STZ in mice fed a HFD. qRT-PCR data showed that there was a significant increase in the mRNA expression of calpain-1 levels in STZ-treated animals of both wild-type ($p=0.023$) and CAST KO ($p=0.005$) compared to those treated with citrate buffer (Fig. 4A, C). Orally administrated SNJ-1945 significantly suppressed the upregulation of gene expression of calpain-1 in both wild-type ($p=0.023$) and CAST KO mice ($p=0.005$) compared to STZ-treated ones, almost bringing them back to normal. However, there was no significant difference in the gene expression of calpain-2 compared to the control in either treated group (Fig. 4B, D). These data showed that gene upregulation of calpain-1, but not calpain-2, was responsible for inducing RGC toxicity in our diabetic model, and that the gene expression of calpain-1 was downregulated by the administration of SNJ-1945.

Cleavage of α-fodrin targeted ganglion cell death was suppressed with SNJ-1945

Since expression of the calpain-1 gene was up-regulated, we tried to determine whether cleaved α-fodrin could be detected in the retina 4-weeks after treatment with STZ. Immunoblot analysis demonstrated that cleaved α-fodrin was significantly increased in STZ-treated wild-type ($p=0.029$) and STZ-treated CAST KO mice ($p=0.024$) compared to a citrate buffer-treated control group (Fig. 5A–B wild-type, C–D CAST KO). We next tried to modify the status of the activated calpain by orally administering SNJ-1945 at 100 mg/kg/day in our diabetic mice. The level of band intensity of cleaved α-fodrin decreased after SNJ-1945 treatment in the wild-type and CAST KO mice ($p=0.981$, 0.937 respectively), approaching the control groups (Figs. 5A–B, C–D). These data suggest that activated calpain-1 in STZ-treated animals led to autolytic cleavage of α-fodrin into its large pro-apoptotic products at 150 kDa, which induced RGC death. SNJ-1945 was able to suppress the band intensity of cleaved fodrin, bringing it close to normal.

Reduction of RGC density and synaptophysin in the diabetic retina was reversed by SNJ-1945

To understand the underlying mechanism of how calpain activation led to RGC degeneration in our diabetic mouse model, having already determined the cause of axonal degeneration, we evaluated the expression of C38 (MB88), an antigen that is specifically expressed in RGCs (Wakabayashi et al., 2010). We also evaluated their cell transduction by examining synaptophysin, a synaptic vesicle protein abundant in the inner retinal neurons (Kurihara et al., 2008). RGC count was significantly decreased in the STZ-treated groups compared to the control citrate buffer groups and STZ-SNJ-1945 groups (Fig. 6A—left panels, C). Interestingly, synaptophysin protein levels also decreased significantly in retinas with hyperglycemia compared to the control (Fig. 6E), especially in the inner plexiform layer (IPL), at the four-week point of the experiment (Fig. 6A—right panels). SNJ-1945 significantly blocked the decrease of synaptophysin protein in the

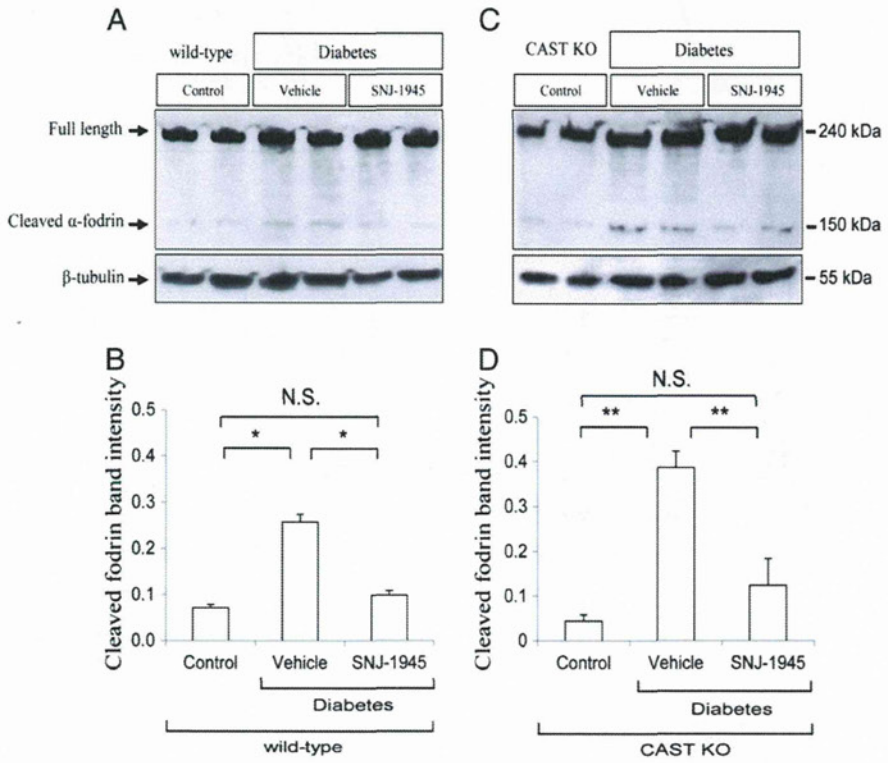

Fig. 5. SNJ-1945 suppressed the cleaved α-fodrin of HFD and STZ-induced hyperglycemia. (A, C) Photographs representing immunoblot analysis. They show the band density of cleaved α-fodrin 4-weeks after the induction of diabetes. (B, D) Quantitative data for the bands representing cleaved fodrin ($n=4$ each group) in wild-type (B) and CAST KO (D) mice. The cleavage of fodrin into its pro-apoptotic products at 150 kDa is generated through the activation of calpain, which was suppressed significantly with SNJ-1945. The density values of cleaved α-fodrin were normalized to density values of β-tubulin. N.S.: no significance. *$p<0.05$, **$p<0.01$ vs. control.

retina (Fig. 6D–E). These data suggested that a loss in synaptic vesicle input might occur in DR, linked to calpain activation. SNJ-1945 administration rescued RGCs and their synapses from diabetic pathological changes.

SNJ-1945 suppresses oxidative stress-induced RGC death in vivo

We next investigated the role of oxidative stress in inducing RGC death, including the role of calpain activation. We induced hyperglycemia

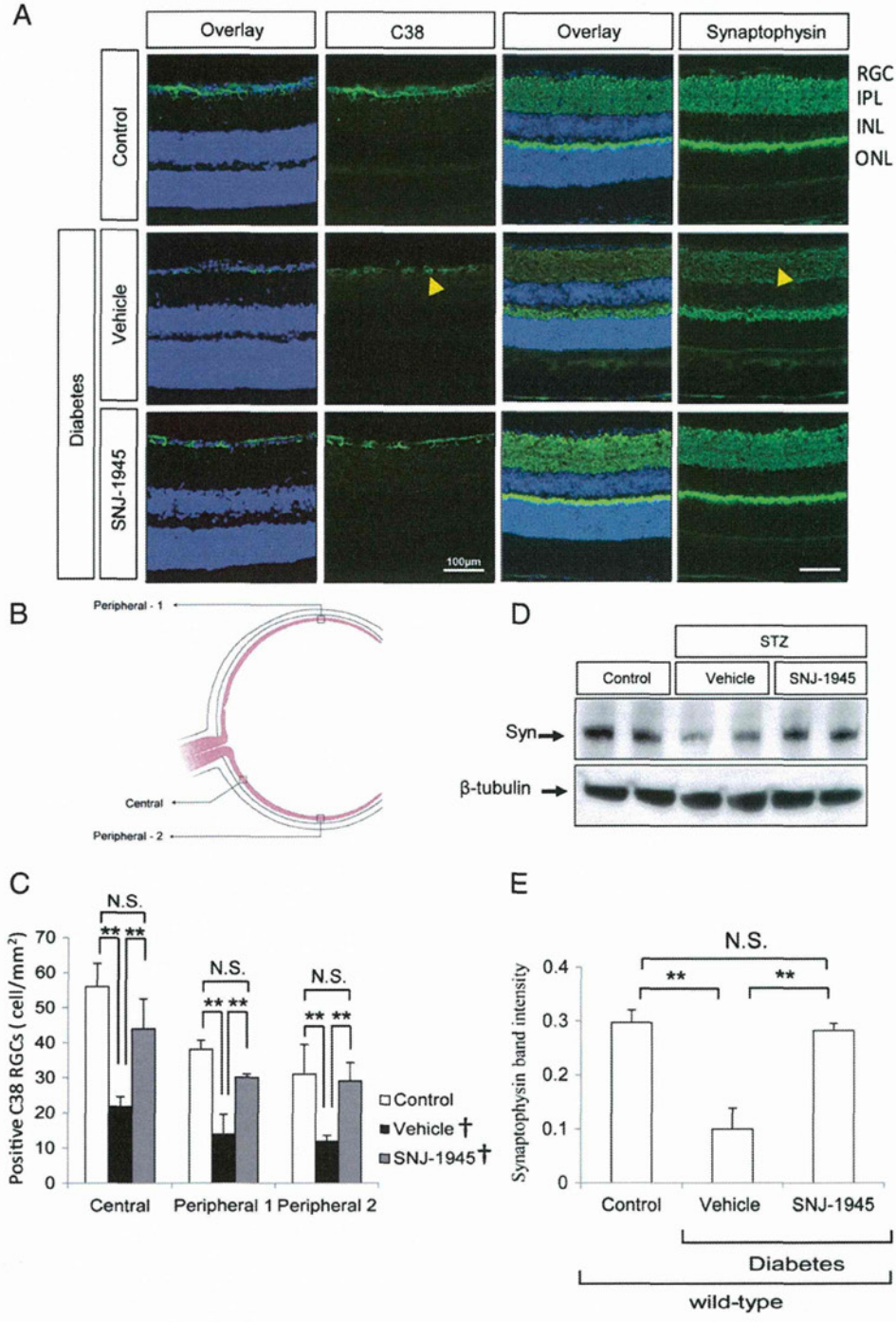

Fig. 6. SNJ-1945 prevented the HFD- and hyperglycemia-induced reduction of RGC and synaptophysin. (A) Representative photomicrographs of retinal sections immunostained with antibody against C38 (upper left panels), synaptophysin (upper right panels) and double labeling (overlap) with DAPI nuclear staining. The yellow arrowheads show a coincident decrease in both positive C38 RGC expression (left middle panel) and synaptophysin (right middle panel), and immunoreactivity in the inner plexiform layer (IPL) in the diabetic mice, compared to those treated with SNJ-1945. (B) Illustrated diagram of a cryosectioned eyecup showing the positions of the microscopic captures. (C) Quantitative data for the number of positive C38 RGCs (n = 16 in each condition). (D) Representative photographs of immunoblot analysis with synaptophysin (Syn: upper panel) and β-actin (lower panel) 4-weeks after induction of diabetes with and without SNJ-1945. (E) Quantitative data for the band intensity ratio of synaptophysin to β-tubulin (n = 4 each condition). The figures show that SNJ-1945 prevented HFD- and hyperglycemia-induced reduction in RGCs and synaptophysin protein. †STZ-treated group, N.S.: no significance. **$p<0.01$ vs. control.

in Nrf2 KO mice fed a HFD and over the course of 4-weeks (Fig. 7). Nrf2 is a key transcript factor for the expression of antioxidant genes, such as glutathione and HO-1, and protects against oxidative stress. Our data showed a significant decrease in the density of FG-labeled RGCs at week four in STZ-treated Nrf2 KO mice (2312 ± 212 cells/mm^2, $p<0.0001$), compared to wild-type mice treated with citrate buffer (3746 ± 115 cells/mm^2) (Fig. 7A–B). The survival rate of RGCs was 58.2% at week four, suggesting that oxidative stress is also involved in the pathogenesis of hyperglycemia-induced RGC death. Since it has been reported that oxidative stress increases intracellular free Ca^{2+} levels, and activates Ca^{2+}-dependent enzymes (Ray et al., 2000), we evaluated calpain status in Nrf2 KO mice retinas at the four week mark of the experiment by investigating the state of α-fodrin. Immunoblot analysis demonstrated that cleaved α-fodrin increased significantly in STZ-treated mice ($p=0.004$) compared to animals treated with the citrate buffer. The cleavage of fodrin was significantly ($p=0.004$) reduced in STZ-treated mice with administration of SNJ-1945 compared to vehicle groups (Fig. 7C–D). Interestingly, SNJ-1945 also significantly suppressed RGC death after just 2-weeks of administration (Fig. 8A–B). These data revealed that oxidative stress is involved in inducing RGC death in our diabetic model, and that SNJ-1945 can significantly suppress RGC degeneration by preventing subsequent calpain activation (Fig. 1).

Hyperglycemia-induced RGC death was mediated by oxidative stress and the SNJ-1945 had a neuroprotective effect in vitro

Measuring free radicals in animal models is difficult because of their transient nature, but since the production of free radicals is closely associated with hyperglycemia in cell culture models (Mullarkey et al., 1990), we tried to evaluate the state of oxidative stress on cultured RGCs (Fig. 9) in a high-glucose culture medium, using an anti-oxidant supplement with or without SNJ-1945. In a high glucose culture medium without an anti-oxidant supplement, the density of surviving βIII-tubulin (+) RGCs decreased significantly ($1.1 \pm 0.5\%$, $p<0.0001$) compared to cultures treated with anti-oxidants ($6.3 \pm 1.2\%$). SNJ-1945 (40 μM) significantly suppressed RGC death ($4.5 \pm 0.3\%$, $p<0.0001$) (Fig. 9A–B). When anti-oxidants and SNJ-1945 were combined, there was a significant ($8.6 \pm 0.6\%$, $p=0.0271$) additive neuro-protective effect compared to cultures treated with only anti-oxidants. These data give clear evidence that calpain and oxidative stress participate in hyperglycemia-induced RGC death. Together, anti-oxidants and calpain inhibitors provide potent neuroprotection against hyperglycemia-induced RGC toxicity.

Discussion

RGCs are the main output neurons in the retinal visual pathway and direct dysfunction of RGCs influences a patient's visual function. Thus, RGCs are an important cellular target for neuro-protective treatment to prevent blindness in patients with DR. This study was designed to investigate the neurotoxic effect on RGCs of combining a high fat diet (HFD; as a source of lipid peroxidation) (Park et al., 2010), and hyperglycemia, induced by frequent low doses of STZ.

Our data showed that a HFD and hyperglycemia caused a significant increase in RGC degeneration, including the synapse and axon, at the four-week mark of the experiment. In CAST KO mice, which

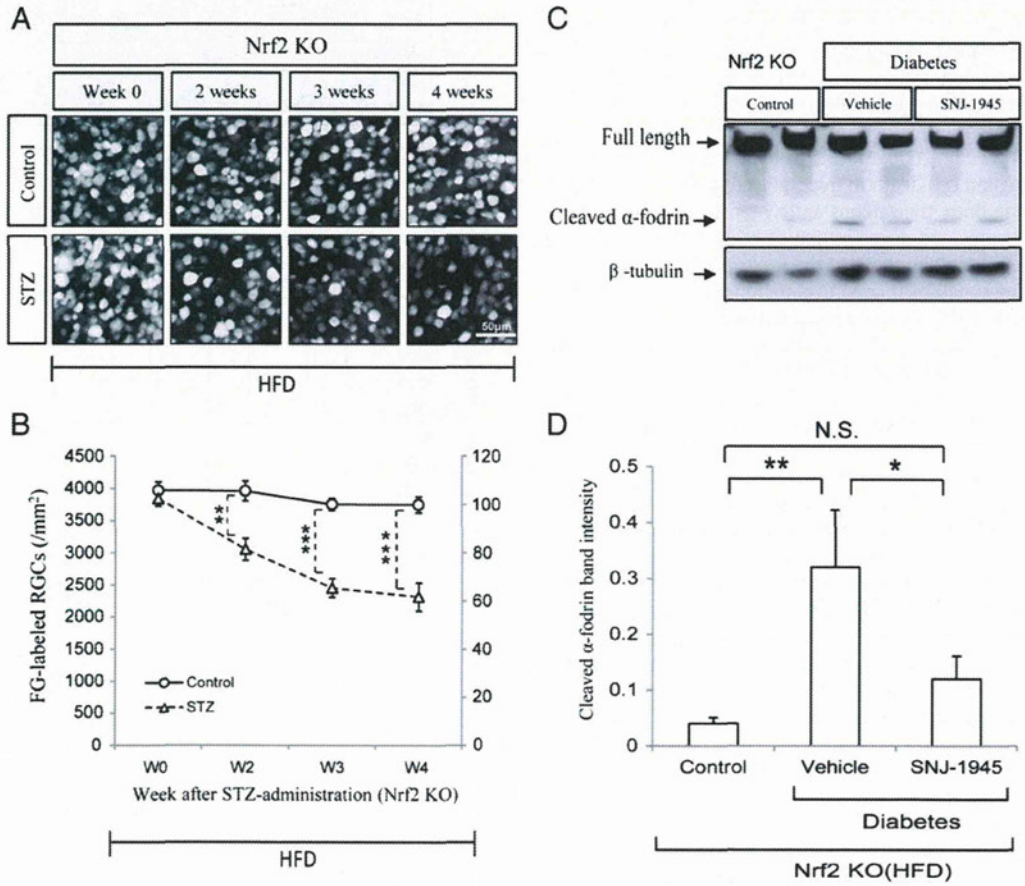

Fig. 7. Nrf2 deficiency in mice treated with STZ induced RGC degeneration; SNJ-1945 prevented cleavage of fodrin. (A) Representative photos of fluorogold (FG)—back labeled RGCs in flat-mounted Nrf2 KO mouse retinas after 4-weeks. (B) Quantitative data for FG-labeled RGCs ($n=6$ each time point). (C) Photographs of immunoblot analysis, showing that band intensity was significantly up-regulated in STZ-treated mice compared to mice treated with citrate buffer and SNJ-1945. (D) Bar chart showing the band density of cleaved fodrin ($n=4$ each group), normalized to the density of β-tubulin. N.S.: no significance, *$p<0.05$, **$p<0.001$, ***$p<0.0001$ vs. control. Circles = control, triangles = STZ.

are susceptible to calpain activation, hyperglycemia-induced RGC death was higher earlier on, at the two-week mark, compared to wild-type mice (Fig. 2B). These results indicate that calpain plays an important role in RGC degeneration.

The percentage of surviving RGCs in wild-type and CAST KO mice is close in week four, but this may be explained as calpastatin showed only a limited, weak neuroprotective effect; it suppressed RGC death during only the first 2-weeks following STZ induction in wild-type mice fed a HFD. Noting this, we attempted to suppress calpain activation by using a more potent exogenous calpain inhibitor, SNJ-1945, an α-ketoamide derivative containing a secondary amine in place of the cyclopropyl ring. This increases the potency of calpain inhibition by ten times (Cuerrier et al., 2006), with the advantage that it can cross the blood–retinal barrier (Shirasaki et al., 2006). However, it shows a protective effect on cultured human retinal endothelial cells (Ma et al., 2009). After induction of hyperglycemia, RGC and axonal degeneration was successfully prevented by SNJ-1945 4-weeks into the experiment (Fig. 3).

It has been reported that mRNA expression of calpain is correlated with its activity (Li et al., 2009; Muroya et al., 2012). SNJ-1945 was able to suppress mRNA overexpression of calpain-1 in our diabetic model (Fig. 4), which may be explained by the changing shape of calpain shifting domains to form an active compact structure, affecting mRNA expression (Suzuki et al., 2004). However, SNJ-1945 prevents these structural changes, and is thus responsible for keeping mRNA expression of calpain-1 close to normal.

A recent publication by our team concluded that orally administered SNJ-1945 protects against RGC degeneration induced by optic nerve crush and vinblastine in an in vivo mouse model (Ryu et al., 2011). Those types of axonal damage induced rapid RGC loss in the first 7-days, with a mitochondrial-dependent cell death pathway as a response to a rapid disintegration and alternation of axoplasmic flow (Knoferle et al., 2010). However, in glaucoma, RGC degenerate specifically from axonal damage in the lamina cribrosa on the optic nerve (Kerrigan-Baumrind et al., 2000). In this study, we tried to explore the mechanism of ganglion cell death in hyperglycemia-induced retinopathy by investigating both, their axons and synapsis. Interestingly, our data had shown a coincided degeneration of RGCs and their synapsis, a synaptic vesicle protein abundant in the inner plexiform layer (IPL), mainly representing synapses related to ganglion cells, and responsible for signal transduction, suggested that impairment on synaptic signal is involved in RGC death in early stages of DR, together with axonal degeneration. However, it is still unclear whether synaptophysin degradation precedes cell body deaths. In any case, oral administration of SNJ-1945 had a significant preventive effect against diabetic changes to RGC synapses (Fig. 6D–E).

In many studies, the common way of assessing the autolytic activity of calpain is through measuring its substrates (α-fodrin), and its break-down end products (Kampfl et al., 1996; Nakazawa et al., 2009; Nath et al., 1996). Our model and data showed that pro-apoptotic end products of cleaved α-fodrin at 150 kDa, which had been up-regulated in STZ-treated wild-type, CAST KO and Nrf2 KO animals, were significantly reduced by oral administration of SNJ-1945 (Fig. 5, 7C–D). This reveals that cleavage of fodrin was involved in the mechanism of RGC death in our diabetic mouse models.

In our investigation of the role of oxidative stress in our experiment, we induced hyperglycemia in Nrf2 KO mice, which are susceptible to oxidative stress. We found that HFD- and hyperglycemia-induced RGC deaths were significantly augmented in Nrf2 KO mice, and decreased significantly by SNJ-1945 (Fig. 7A–B, 8 A–B). Previous reports have documented that oxidative stress increases intracellular free Ca^{2+} levels, and activates Ca^{2+}-dependent enzymes (Ray et al., 2000). In response, we evaluated the link, if any, between oxidative stress and calpain activation in a high glucose culture medium with or without antioxidants in an in vitro retinal experimental model (Fig. 9). Our data has shown a significant neurodegenerative influence of RGCs 24 hr after incubation in a high glucose (45 mM D-glucose) culture without antioxidant (AO−), compared to those treated with antioxidant supplement (AO+). These results suggested that oxidative stress was induced in high glucose culture medium and participated in pathogenesis of RGCs death. Then, we evaluated the condition of the high glucose culture medium with (40 μM) SNJ-1945. It has significantly protected RGCs against high glucose-induced oxidative stress, when compared to the non-treated groups (Fig. 9B). The neuroprotective effect of SNJ-1945 was weaker than that of the antioxidants in vitro because the antioxidants were a mixture of potent antioxidant compounds. This does not imply that activation of the calpain-signal was not involved in the RGC death. However, the influence which SNJ-1945 inhibits in high-glucose conditions, and in the presence of antioxidants, may be a remnant of oxidative stress that has not been canceled by the antioxidants, or may be another cell death pathway (i.e. ER stress). These data suggest that

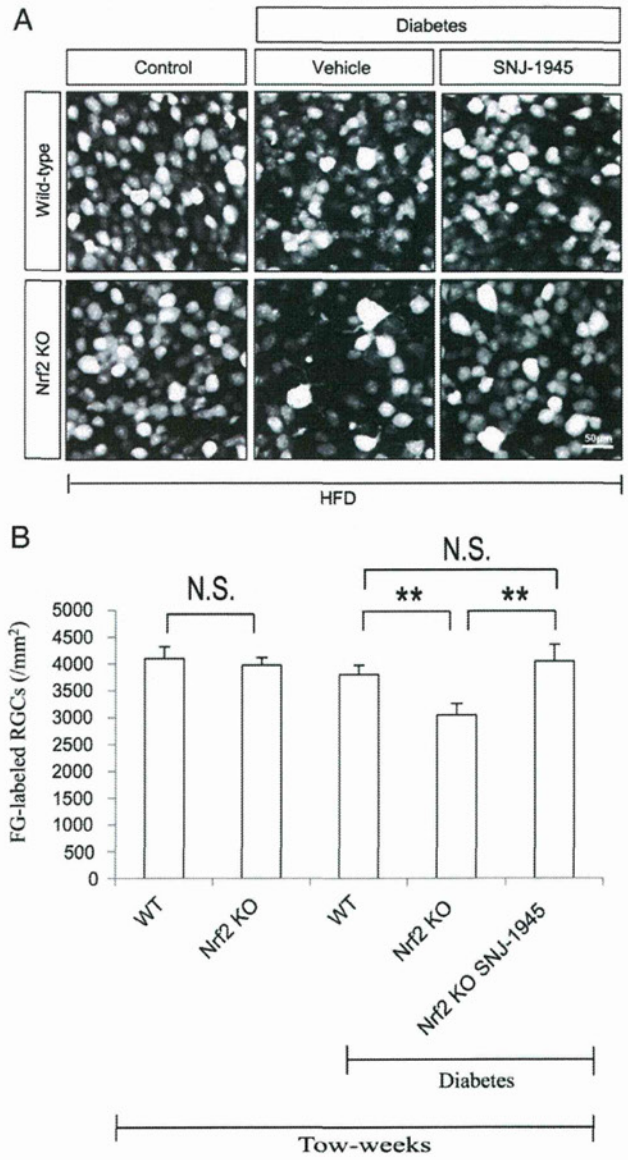

Fig. 8. SNJ-1945 suppressed oxidative stress induced RGC-degeneration in vivo. (A) Representative photos of positive FG-labeled RGCs in flat-mounted retinas, showing a dramatic decrease in RGCs in diabetic Nrf2 KO mice compared to non-diabetic wild-type mice. (B) Quantitative data of FG-labeled RGC density showing a significant degeneration in number of RGCs compared to wild-type and Nrf2 KO SNJ-1945-treated mice 2-weeks after STZ-induced hyperglycemia. Data represented mean ± SEM. N.S.: no significance. **$p < 0.001$ vs. control.

oxidative stress induced by hyperglycemia is involved in the pathogenesis of RGC death, and that calpain inhibitors have the potential to protect RGCs against hyperglycemia-induced RGC toxicity.

At the cellular level, the mechanism of RGC death in our diabetic model is hypothesized to be due to hyper-excitability of the cell membrane, which occurs in hyperglycemia and leads to cell membrane depolarization and a Ca^{2+} influx through the voltage sensitive Ca^{2+} channel. Once inside the cell, the excitation of ER and mitochondria through an increase in oxidative stress hints at a release of more intracellular Ca^{2+}. Subsequently, calpain activation and cleavage of α-fodrin into pro-apoptotic end products will lead to cell deaths (Fig. 1).

In conclusion, calpain plays a curtailed role in HFD-induced RGC death caused by hyperglycemia and oxidative stress. Inhibition of calpain and the administration of antioxidants have the potential to prevent neuronal dysfunction in the early stages of vision threatening DR.

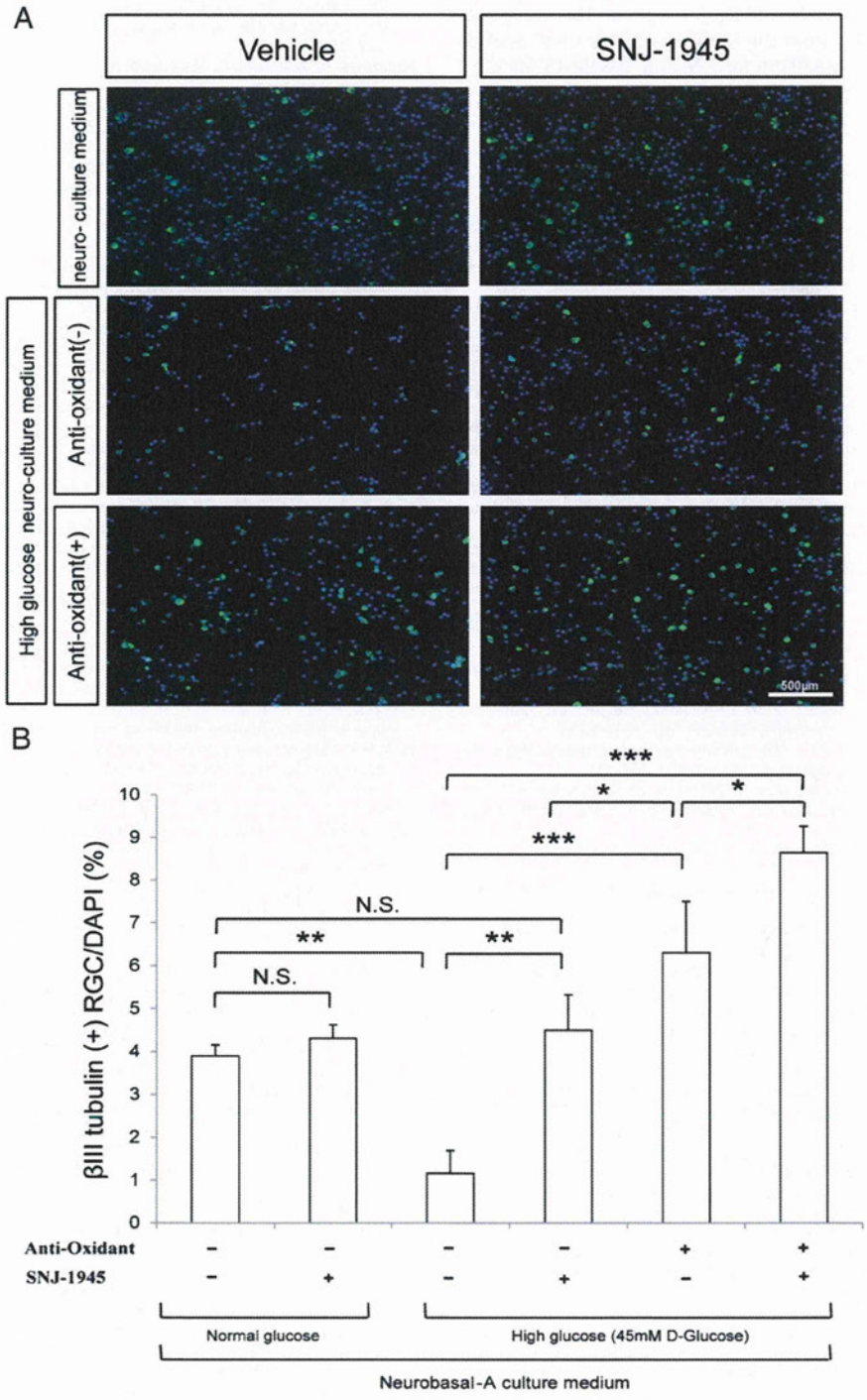

Fig. 9. Hyperglycemia-induced RGC death was mediated by oxidative stress and the neuro-protective effect of SNJ-1945 in vitro. (A) Representative photomicrographs of βIII tubulin-positive RGCs, normal sugar neurobasal-A culture medium with or without SNJ-1945 (upper panels). High sugar (45 mM D-glucose) neurobasal-A culture medium without anti-oxidant (middle panels) or with anti-oxidant (lower panels). SNJ-1945 (40 μM in final) was added to the groups on the right, and 0.1% DMSO to the vehicle. (B) Quantitative data for surviving RGCs 24 hr after culture (% of βIII tubulin-positive RGCs to DAPI). Data represented mean ± SEM. N.S.: no significance. *$p<0.05$, **$p<0.01$, ***$p<0.001$ vs. control.

Supplementary data to this article can be found online at http://dx.doi.org/10.1016/j.nbd.2012.07.025.

Acknowledgments

We thank Mr. Tim Hilts for reviewing and editing the language of the manuscript, Mr. Kohtaro Yamamoto and Ms. Kaori Abe for the technical assistance, and the experimental research laboratories at Tohoku University Medical School. The C38 antibody was kindly gifted by Dr. Takatoshi Wakabayashi and Dr. Jun Kosaka. This study was supported by Grants-in-Aid from the Ministry of Education, Science and Technology of Japan (24659756 for T.N. and 40625513 for Y.T.), Santan Pharmaceutical Founder Commemoration Ophthalmic Research Fund, and Japanese National Society for the Prevention of Blindness (T.N.).

References

Abu-El-Asrar, A.M., Dralands, L., Missotten, L., Al-Jadaan, I.A., Geboes, K., 2004. Expression of apoptosis markers in the retinas of human subjects with diabetes. Invest. Ophthalmol. Vis. Sci. 45, 2760–2766.

Camins, A., Verdaguer, E., Folch, J., Pallas, M., 2006. Involvement of calpain activation in neurodegenerative processes. CNS Drug Rev. 12, 135–148.

Chihara, E., Matsuoka, T., Ogura, Y., Matsumura, M., 1993. Retinal nerve-fiber layer defect as an early manifestation of diabetic-retinopathy. Ophthalmology 100, 1147–1151.

Costa, V.P., de Faria, J.M.L., Russ, H., 2002. Retinal nerve fibre layer loss in patients with type 1 diabetes mellitus without retinopathy. Br. J. Ophthalmol. 86, 725–728.

Cuerrier, D., Moldoveanu, T., Inoue, J., Davies, P.L., Campbell, R.L., 2006. Calpain inhibition by alpha-ketoamide and cyclic hemiacetal inhibitors revealed by X-ray crystallography. Biochemistry 45, 7446–7452.

Fong, D.S., Aiello, L., Gardner, T.W., King, G.L., Blankenship, G., Cavallerano, J.D., Ferris III, F.L., Klein, R., American Diabetes A., 2004. Retinopathy in diabetes. Diabetes Care 27 (Suppl. 1), S84–S87.

Frishman, L.J., Shen, F.F., Du, L., Robson, J.G., Harwerth, R.S., Smith III, E.L., Carter-Dawson, L., Crawford, M.L., 1996. The scotopic electroretinogram of macaque after retinal ganglion cell loss from experimental glaucoma. Invest. Ophthalmol. Vis. Sci. 37, 125–141.

Goll, D.E., Thompson, V.F., Li, H., Wei, W., Cong, J., 2003. The calpain system. Physiol. Rev. 83, 731–801.

Hancock, H.A., Kraft, T.W., 2004. Oscillatory potential analysis and ERGs of normal and diabetic rats. Invest. Ophthalmol. Vis. Sci. 45, 1002–1008.

Hanna, R.A., Garcia-Diaz, B.E., Davies, P.L., 2007. Calpastatin simultaneously binds four calpains with different kinetic constants. FEBS Lett. 581, 2894–2898.

Hanna, R.A., Campbell, R.L., Davies, P.L., 2008. Calcium-bound structure of calpain and its mechanism of inhibition by calpastatin. Nature 456, 409–412.

Hinokio, Y., Suzuki, S., Hirai, M., Chiba, M., Hirai, A., Toyota, T., 1999. Oxidative DNA damage in diabetes mellitus: its association with diabetic complications. Diabetologia 42, 995–998.

Hu, F.B., 2011. Globalization of diabetes: the role of diet, lifestyle, and genes. Diabetes Care 34, 1249–1257.

Huang, Y., Wang, K.K., 2001. The calpain family and human disease. Trends Mol. Med. 7, 355–362.

Itoh, K., Chiba, T., Takahashi, S., Ishii, T., Igarashi, K., Katoh, Y., Oyake, T., Hayashi, N., Satoh, K., Hatayama, I., Yamamoto, M., Nabeshima, Y., 1997. An Nrf2/small Maf heterodimer mediates the induction of phase II detoxifying enzyme genes through antioxidant response elements. Biochem. Biophys. Res. Commun. 236, 313–322.

Itoh, K., Wakabayashi, N., Katoh, Y., Ishii, T., Igarashi, K., Engel, J.D., Yamamoto, M., 1999. Keap1 represses nuclear activation of antioxidant responsive elements by Nrf2 through binding to the amino-terminal Neh2 domain. Genes Dev. 13, 76–86.

Kampfl, A., Posmantur, R., Nixon, R., Grynspan, F., Zhao, X., Liu, S.J., Newcomb, J.K., Clifton, G.L., Hayes, R.L., 1996. mu-Calpain activation and calpain-mediated cytoskeletal proteolysis following traumatic brain injury. J. Neurochem. 67, 1575–1583.

Kerrigan-Baumrind, L.A., Quigley, H.A., Pease, M.E., Kerrigan, D.F., Mitchell, R.S., 2000. Number of ganglion cells in glaucoma eyes compared with threshold visual field tests in the same persons. Invest. Ophthalmol. Vis. Sci. 41, 741–748.

Kizawa, J., Machida, S., Kobayashi, T., Gotoh, Y., Kurosaka, D., 2006. Changes of oscillatory potentials and photopic negative response in patients with early diabetic retinopathy. Jpn. J. Ophthalmol. 50, 367–373.

Knoferle, J., Koch, J.C., Ostendorf, T., Michel, U., Planchamp, V., Vutova, P., Tonges, L., Stadelmann, C., Bruck, W., Bahr, M., Lingor, P., 2010. Mechanisms of acute axonal degeneration in the optic nerve in vivo. Proc. Natl. Acad. Sci. U. S. A. 107, 6064–6069.

Kurihara, T., Ozawa, Y., Nagai, N., Shinoda, K., Noda, K., Imamura, Y., Tsubota, K., Okano, H., Oike, Y., Ishida, S., 2008. Angiotensin II type 1 receptor signaling contributes to synaptophysin degradation and neuronal dysfunction in the diabetic retina. Diabetes 57, 2191–2198.

Li, Z., Cao, B., Zhao, B., Yang, X., Fan, M.Z., Yang, J., 2009. Decreased expression of calpain and calpastatin mRNA during development is highly correlated with muscle protein accumulation in neonatal pigs. Comp. Biochem. Physiol. A Mol. Integr. Physiol. 152, 498–503.

Ma, H., Tochigi, A., Shearer, T.R., Azuma, M., 2009. Calpain inhibitor SNJ-1945 attenuates events prior to angiogenesis in cultured human retinal endothelial cells. J. Ocul. Pharmacol. Ther. 25, 409–414.

Mu, J., Woods, J., Zhou, Y.P., Roy, R.S., Li, Z., Zycband, E., Feng, Y., Zhu, L., Li, C., Howard, A.D., Moller, D.E., Thornberry, N.A., Zhang, B.B., 2006. Chronic inhibition of dipeptidyl peptidase-4 with a sitagliptin analog preserves pancreatic beta-cell mass and function in a rodent model of type 2 diabetes. Diabetes 55, 1695–1704.

Mullarkey, C.J., Edelstein, D., Brownlee, M., 1990. Free radical generation by early glycation products: a mechanism for accelerated atherogenesis in diabetes. Biochem. Biophys. Res. Commun. 173, 932–939.

Muroya, S., Neath, K.E., Nakajima, I., Oe, M., Shibata, M., Ojima, K., Chikuni, K., 2012. Differences in mRNA expression of calpains, calpastatin isoforms and calpain/calpastatin ratios among bovine skeletal muscles. Anim. Sci. J. 83, 252–259.

Nakazawa, T., Nakazawa, C., Matsubara, A., Noda, K., Hisatomi, T., She, H., Michaud, N., Hafezi-Moghadam, A., Miller, J.W., Benowitz, L.I., 2006. Tumor necrosis factor-alpha mediates oligodendrocyte death and delayed retinal ganglion cell loss in a mouse model of glaucoma. J. Neurosci. 26, 12633–12641.

Nakazawa, T., Takahashi, H., Nishijima, K., Shimura, M., Fuse, N., Tamai, M., Hafezi-Moghadam, A., Nishida, K., 2007a. Pitavastatin prevents NMDA-induced retinal ganglion cell death by suppressing leukocyte recruitment. J. Neurochem. 100, 1018–1031.

Nakazawa, T., Takeda, M., Lewis, G.P., Cho, K.S., Jiao, J., Wilhelmsson, U., Fisher, S.K., Pekny, M., Chen, D.F., Miller, J.W., 2007b. Attenuated glial reactions and photoreceptor degeneration after retinal detachment in mice deficient in glial fibrillary acidic protein and vimentin. Invest. Ophthalmol. Vis. Sci. 48, 2760–2768.

Nakazawa, T., Hisatomi, T., Nakazawa, C., Noda, K., Maruyama, K., She, H., Matsubara, A., Miyahara, S., Nakao, S., Yin, Y., Benowitz, L., Hafezi-Moghadam, A., Miller, J.W., 2007c. Monocyte chemoattractant protein 1 mediates retinal detachment-induced photoreceptor apoptosis. Proc. Natl. Acad. Sci. U. S. A. 104, 2425–2430.

Nakazawa, T., Shimura, M., Ryu, M., Nishida, K., Pages, G., Pouyssegur, J., Endo, S., 2008. ERK1 plays a critical protective role against N-methyl-D-aspartate-induced retinal injury. J. Neurosci. Res. 86, 136–144.

Nakazawa, T., Shimura, M., Mourin, R., Kondo, M., Yokokura, S., Saido, T.C., Nishida, K., Endo, S., 2009. Calpain-mediated degradation of G-substrate plays a critical role in retinal excitotoxicity for amacrine cells. J. Neurosci. Res. 87, 1412–1423.

Nath, R., Raser, K.J., Stafford, D., Hajimohammadreza, I., Posner, A., Allen, H., Talanian, R.V., Yuen, P., Gilbertsen, R.B., Wang, K.K., 1996. Non-erythroid alpha-spectrin breakdown by calpain and interleukin 1 beta-converting-enzyme-like protease(s) in apoptotic cells: contributory roles of both protease families in neuronal apoptosis. Biochem. J. 319 (Pt 3), 683–690.

Oka, T., Walkup, R.D., Tamada, Y., Nakajima, E., Tochigi, A., Shearer, T.R., Azuma, M., 2006. Amelioration of retinal degeneration and proteolysis in acute ocular hypertensive rats by calpain inhibitor ((1S)-1-((((1S)-1-benzyl-3-cyclopropylamino-2,3-di-oxopropyl)amino)carbony l)-3-methylbutyl)carbamic acid 5-methoxy-3-oxapentyl ester. Neuroscience 141, 2139–2145.

Pan, H.Z., Zhang, H., Chang, D., Li, H., Sui, H., 2008. The change of oxidative stress products in diabetes mellitus and diabetic retinopathy. Br. J. Ophthalmol. 92, 548–551.

Park, H.R., Park, M., Choi, J., Park, K.Y., Chung, H.Y., Lee, J., 2010. A high-fat diet impairs neurogenesis: involvement of lipid peroxidation and brain-derived neurotrophic factor. Neurosci. Lett. 482, 235–239.

Perrin, B.J., Huttenlocher, A., 2002. Calpain. Int. J. Biochem. Cell Biol. 34, 722–725.

Ray, S.K., Fidan, M., Nowak, M.W., Wilford, G.G., Hogan, E.L., Banik, N.L., 2000. Oxidative stress and Ca2+ influx upregulate calpain and induce apoptosis in PC12 cells. Brain Res. 852, 326–334.

Resnikoff, S., Pascolini, D., Etya'ale, D., Kocur, I., Pararajasegaram, R., Pokharel, G.P., Mariotti, S.P., 2004. Global data on visual impairment in the year 2002. Bull. World Health Organ. 82, 844–851.

Ryu, M., Yasuda, M., Shi, D., Shanab, A.Y., Watanabe, R., Himori, N., Omodaka, K., Yokoyama, Y., Takano, J., Saido, T., Nakazawa, T., 2011. Critical role of calpain in axonal damage-induced retinal ganglion cell death. J. Neurosci. Res.

Sano, T., Umeda, F., Hashimoto, T., Nawata, H., Utsumi, H., 1998. Oxidative stress measurement by in vivo electron spin resonance spectroscopy in rats with streptozotocin-induced diabetes. Diabetologia 41, 1355–1360.

Shaw, J.E., Sicree, R.A., Zimmet, P.Z., 2010. Global estimates of the prevalence of diabetes for 2010 and 2030. Diabetes Res. Clin. Pract. 87, 4–14.

Shirasaki, Y., Miyashita, H., Yamaguchi, M., Inoue, J., Nakamura, M., 2005. Exploration of orally available calpain inhibitors: peptidyl alpha-ketoamides containing an amphiphile at P3 site. Bioorg. Med. Chem. 13, 4473–4484.

Shirasaki, Y., Yamaguchi, M., Miyashita, H., 2006. Retinal penetration of calpain inhibitors in rats after oral administration. J. Ocul. Pharmacol. Ther. 22, 417–424.

Srinivasan, K., Viswanad, B., Asrat, L., Kaul, C.L., Ramarao, P., 2005. Combination of high-fat diet-fed and low-dose streptozotocin-treated rat: a model for type 2 diabetes and pharmacological screening. Pharmacol. Res. 52, 313–320.

Stys, P.K., Jiang, Q., 2002. Calpain-dependent neurofilament breakdown in anoxic and ischemic rat central axons. Neurosci. Lett. 328, 150–154.

Suzuki, K., Hata, S., Kawabata, Y., Sorimachi, H., 2004. Structure, activation, and biology of calpain. Diabetes 53 (Suppl. 1), S12–S18.

Takano, J., Tomioka, M., Tsubuki, S., Higuchi, M., Iwata, N., Itohara, S., Maki, M., Saido, T.C., 2005. Calpain mediates excitotoxic DNA fragmentation via mitochondrial pathways in adult brains: evidence from calpastatin mutant mice. J. Biol. Chem. 280, 16175–16184.

Wakabayashi, T., Kosaka, J., Mochii, M., Miki, Y., Mori, T., Takamori, Y., Yamada, H., 2010. C38, equivalent to BM88, is developmentally expressed in maturing retinal neurons and enhances neuronal maturation. J. Neurochem. 112, 1235–1248.

Intraocular Concentrations of Cytokines and Chemokines in Rhegmatogenous Retinal Detachment and the Effect of Intravitreal Triamcinolone Acetonide

HIROSHI KUNIKATA, MASAYUKI YASUDA, NAOKO AIZAWA, YUJI TANAKA, TOSHIAKI ABE, AND TORU NAKAZAWA

• PURPOSE: To investigate the role of intravitreal injection of triamcinolone acetonide (IVTA) in preventing photoreceptor apoptosis in eyes with rhegmatogenous retinal detachment (RRD) by measuring cytokine levels in the aqueous humor before and after IVTA.

• DESIGN: Prospective, nonrandomized, interventional case series.

• METHODS: SETTING: Institutional. PATIENTS: Nineteen eyes of 19 consecutive patients with RRD. INTERVENTION: All 19 eyes underwent IVTA 1 day before 25-gauge vitrectomy. Seventeen eyes free of retinal vascular disease served as controls. MAIN OUTCOME MEASURE: Both baseline and 1 day post-IVTA measurements were made of the relative concentrations of 15 soluble factors (3 cytokines, 7 chemokines, and 5 growth factors). The associations with clinical findings, including macular status, were then analyzed.

• RESULTS: Elevated monocyte chemotactic protein 1 (MCP-1), macrophage inflammatory protein 1β (MIP-1β), and interferon γ–induced protein 10 (IP-10) in eyes with RRD were significantly reduced after IVTA. MCP-1 levels were significantly correlated with MIP-1β and IP-10 before and after IVTA. The decreases in MCP-1, MIP-1β, and IP-10 were also closely correlated to each other. Both before and after IVTA, MCP-1 was higher in eyes with macula-off RRD than in eyes with macula-on RRD.

• CONCLUSIONS: IVTA suppressed elevated levels of intraocular MCP-1, MIP-1β, and IP-10 in eyes with RRD. The decrease in the aqueous levels of each of these factors was significantly correlated with the others. In addition to MCP-1, MIP-1β and IP-10 might potentially be additional target molecules for RRD therapy. (Am J Ophthalmol 2013;155:1028–1037. © 2013 by Elsevier Inc. All rights reserved.)

Accepted for publication Jan 8, 2013.

From the Department of Ophthalmology (H.K., M.Y., N.A., Y.T., T.N.) and Division of Clinical Cell Therapy (T.A.), Tohoku University Graduate School of Medicine, Sendai, Japan.

Inquiries to Hiroshi Kunikata, Department of Ophthalmology, Tohoku University Graduate School of Medicine, 1-1 Seiryo-machi, Aoba-ku, Sendai 980-8574, Japan; e-mail: kunikata@oph.med.tohoku.ac.jp

RHEGMATOGENOUS RETINAL DETACHMENT (RRD) IS a common retinal disease that causes visual field defects and severe visual disturbance. Newly developed surgical interventions, particularly 25-gauge microincision vitrectomy surgery (25GMIVS), have led to a very high initial reattachment rate for eyes with RRD, currently about 95%.[1–10] Even after successful reattachment, however, degeneration of the photoreceptors in the detached area of the retina often prevents complete recovery of visual function.[1,11]

Vitreous samples from eyes with RRD have shown significantly elevated levels of monocyte chemotactic protein 1 (MCP-1) compared to controls.[12,13] Previous research by our team, performed with an experimental animal model, showed that MCP-1, along with tumor necrosis factor α (TNF-α), is implicated in the pathogenesis of photoreceptor degeneration and apoptosis following retinal detachment.[14–16] Furthermore, the administration of antibodies and corticosteroid suppressed photoreceptor degeneration and apoptosis in our animal model and lowered the intraocular expression of both MCP-1 and TNF-α. The current study examines the specific effects of corticosteroid in human subjects with RRD. Corticosteroid is already in wide use for a variety of ocular diseases, and triamcinolone acetonide (TA) in particular is well recognized for its anti-inflammatory properties. There are many reports on the successful use of intravitreal injection of triamcinolone acetonide (IVTA) as a treatment for exudative conditions of the posterior segment.[17–25]

In this prospective study, therefore, we hypothesized that in the preoperative period, IVTA would suppress inflammation and photoreceptor apoptosis in human eyes with RRD. To evaluate our hypothesis, we measured levels of intraocular mediators including chemokines and cytokines, such as MCP-1 and TNF-α, and analyzed their response to IVTA in eyes with RRD. Thus, the purpose of this report is to evaluate the effect of IVTA on the intraocular concentration of mediators in eyes with RRD.

MATERIALS AND METHODS

• SETTING AND DESIGN: This was an institutional, prospective, nonrandomized, interventional case series.

0002-9394/$36.00
http://dx.doi.org/10.1016/j.ajo.2013.01.013